

A New Quantum Limit on Laser Linewidth

Chenxu Liu, Maria Mucci, Xi Cao, M. V. Gurudev Dutt, Michael Hatridge, and David Pekker
*Department of Physics and Astronomy, University of Pittsburgh, Pittsburgh, PA, 15260, USA and
Pittsburgh Quantum Institute, University of Pittsburgh, Pittsburgh, PA, 15260, USA*
(Dated: May 27, 2022)

Due to their high coherence, Lasers are a ubiquitous tool in science. The standard quantum limit for the phase coherence time was first introduced by [1], who showed that the minimum possible laser linewidth is determined by the linewidth of the laser cavity divided by twice the number of photons in the cavity. Later, Wiseman showed theoretically that by using Susskind-Glogower operators [2] to couple the gain medium to the laser cavity it is possible to eliminate pump noise, but not loss noise [3]. This decreases the minimum laser linewidth, though only by a factor of two [4]. In this article, we show that by engineering the coupling between the laser cavity and the output port it is possible to eliminate most of the loss noise as well and construct a laser that has a vastly narrower linewidth, narrower than the standard quantum limit by a factor equal to the number of photons in the laser cavity. We establish a roadmap for building such a device in the laboratory by using Josephson junctions and linear circuit elements to build coupling circuits that behave like Susskind-Glogower operators for a range of cavity photon occupancies and using them to couple the laser cavity to both the gain medium and the output port. This device could be an ultra-coherent, cryogenic light source for microwave quantum information experiments. Further, our laser provides highly squeezed light and could be modified to provide designer quantum light which is an important resource for continuous variable/linear optical quantum computing [5–7], readout of quantum states in superconducting quantum computers [8, 9], quantum metrology [10–13], and quantum communication [14–17]. Finally, our proposal relies on the tools and elements of superconducting quantum information, and thus is a clear example of how quantum engineering techniques can inspire us to re-imagine the limits of conventional quantum systems such as the laser.

The main components of a laser, depicted in Fig. 1, are (1) one or more atoms with an inverted population (also called the gain medium), (2) an atom-cavity coupler, (3) a lasing cavity, (4) a cavity-output coupler and an output transmission line. Previous work on laser theory [4], quantum-cascade lasers [18], superradiant lasers [19], and number-squeezed lasers [20] has focused on the gain medium (1) and the atom-cavity coupler (2). The focus of this paper is making the additional

step of modifying the cavity-output coupler (4), which we show is key to minimizing the phase noise in the lasing cavity.

At optical frequencies, the inherent light-matter coupling is rather weak and consequently optical devices tend to be only weakly nonlinear. Over the past two decades, significant progress has been made on building strongly nonlinear optics. At optical frequencies, strong coupling can be achieved in cavity QED systems by using a cavity to extend the time for light-matter interaction [21]. On the other hand, at microwave frequencies, circuit QED achieves extremely strong light-artificial atom interactions by utilizing the extreme nonlinearity and small size (compared to microwave-frequency photons) of Josephson junctions [22]. Circuit QED devices include the various flavors of superconducting quantum computing platforms with components like fluxonium [23] and transmon qubits [24, 25], resonant cavities, microwave waveguides, and quantum limited parametric amplifiers [26, 27]. There is also experimental precedent for building conventional lasers using superconducting circuits with linear couplers [28–30], as well as devices based on parametrically driven, weakly nonlinear oscillators [31, 32].

The starting point for our exploration is a proposal due to Wiseman [4] for reducing laser spectral linewidth. Wiseman proposed using ‘bare’ (so called because they lack a photon-number scaling pre-factor) raising and lowering operators

$$\hat{e} = \sum_i |i\rangle\langle i+1| \quad \hat{e}^\dagger = \sum_i |i+1\rangle\langle i|, \quad (1)$$

which were first introduced by Susskind and Glogower [2], to couple atoms of the gain medium to the resonant cavity of the laser. As these operators commute with the phase $\hat{\phi}$ of the optical field in the cavity (which can be verified by observing that $\hat{e} = e^{i\hat{\phi}}$), Wiseman’s proposal eliminates pump noise and therefore reduces the minimum linewidth by a factor of two below the standard quantum limit, also known as the Schawlow-Townes (ST) limit.

Our first main result is taking this idea further and applying Wiseman’s scheme to both atom-cavity and cavity-output channel couplings thereby eliminating both pump and cavity loss noise. We term this form of (purely theoretical) laser the Susskind-Glogower Bare Operator (SGBO) laser. While in practice, we must also add some conventional loss to the laser in order to stabilize it, the result is a linewidth that is $\langle n \rangle$ times narrower than the ST limit! Having a mathematical scheme for building an

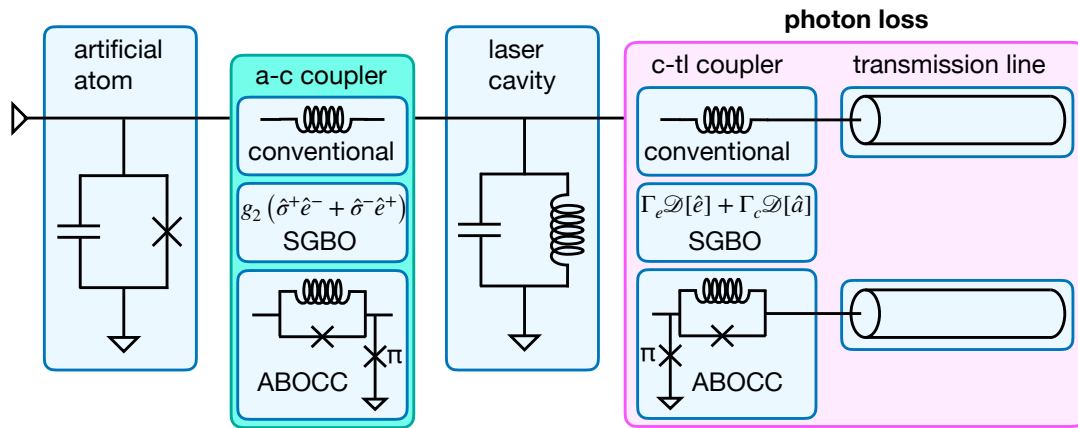


FIG. 1. Schematic of the circuit QED Josephson laser composed of: an artificial two-level atom (transmon qubit) that is incoherently pumped from the ground to the excited state at the rate Γ_p , an atom-cavity (a-c) coupling circuit, a laser cavity made of an LC resonator, a cavity-transmission line (c-tl) coupling circuit, and an output transmission line. The coupling circuits come in three flavors: (1) conventional: linear inductors, (2) Susskind-Glogower 'bare' operator (SGBO) couplers, and (3) Approximate Bare Operator Coupling Circuits (ABOCC). As the SGBO scheme is a purely theoretical construct, it is represented by the a-c coupling Hamiltonian and the photon loss operator.

ultranarrow linewidth laser, we still need an experimentally viable method for building bare operators.

Our second result is an Approximate Bare Operator Coupling Circuit (ABOCC), composed of Josephson junctions and inductors, that approximates the desired coupling Hamiltonian over a range of cavity photon occupancies. For laser applications, our ABOCC is an attractive alternative to previous proposals to build bare operators that relied on adiabatic rapid passage [4, 33–37] as it doesn't require additional drives. We argue that an ABOCC laser, in which couplers are ABOCCs, is a practical laser design that achieves the ultranarrow linewidth promised by SGBO laser. In the remainder of this paper, we first calculate the behavior of the purely theoretical SGBO laser compared to an ideal conventional laser, and then describe the physically realizable ABOCC in detail and describe the potential performance of a laser based on pair of ABOCCs.

In order to compare the linewidth D of different laser designs to the Schawlow-Townes limit D_{ST} we need to generalize the Schawlow-Townes formula for the cases in which the cavity-transmission line coupler is not linear. We do so by replacing the cavity linewidth Γ_c by the ratio of the laser luminosity to the energy of the photons in the cavity $\Gamma_c \rightarrow P_{out}/(\hbar\omega_c\langle n \rangle)$ thus obtaining the formula

$$D_{ST} = \frac{P_{out}}{4\hbar\omega_c\langle n \rangle^2}. \quad (2)$$

For conventional lasers, Eq. (2) is identical to the standard Schawlow-Townes linewidth formula. To ensure that each type of laser is performing at its optimal, we fix the mean photon number in the cavity and minimize the ratio D/D_{ST} by tuning the laser parameters. For example, for the case of the conventional laser, we tune the atom-cavity coupling strength ratio g/Γ_c and the atom incoherent pump rate ratio Γ_p/Γ_c .

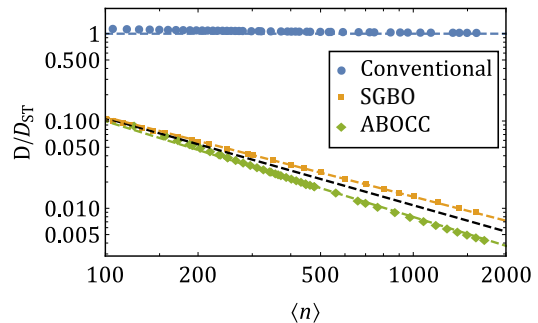


FIG. 2. Laser linewidth (in units of the generalized Schawlow-Townes linewidth) as a function of the average number of photons ($\langle n \rangle$) in the laser cavity for conventional, Susskind-Glogower Bare Operator (SGBO), and Approximately Bare Operator Coupling Circuit (ABOCC) lasers. Engineering of the atom-cavity coupling and the photon loss allows both the SGBO and the ABOCC lasers to achieve a linewidth significantly narrower than the best conventional laser.

In Fig. 2 we plot the optimum laser linewidth, relative to the ST limit, as a function of the average number of photons in the laser cavity for three types of lasers: the conventional laser, the SGBO laser, and the ABOCC laser. All data in this figure was obtained numerically using the spectral method to analyze the master equation (see methods). We observe that for the conventional laser, the ratio D/D_{ST} approaches unity as n becomes large. At the same time, we observe that the laser linewidth for the SGBO laser as well as the ABOCC laser is significantly narrower and goes as $D \sim D_{ST}/\langle n \rangle$.

We start by extending Wiseman's strategy for decreasing the laser linewidth to make the SGBO laser. Following Wiseman, we replace the linear inductive coupling between the atom and the cavity by the bare operator

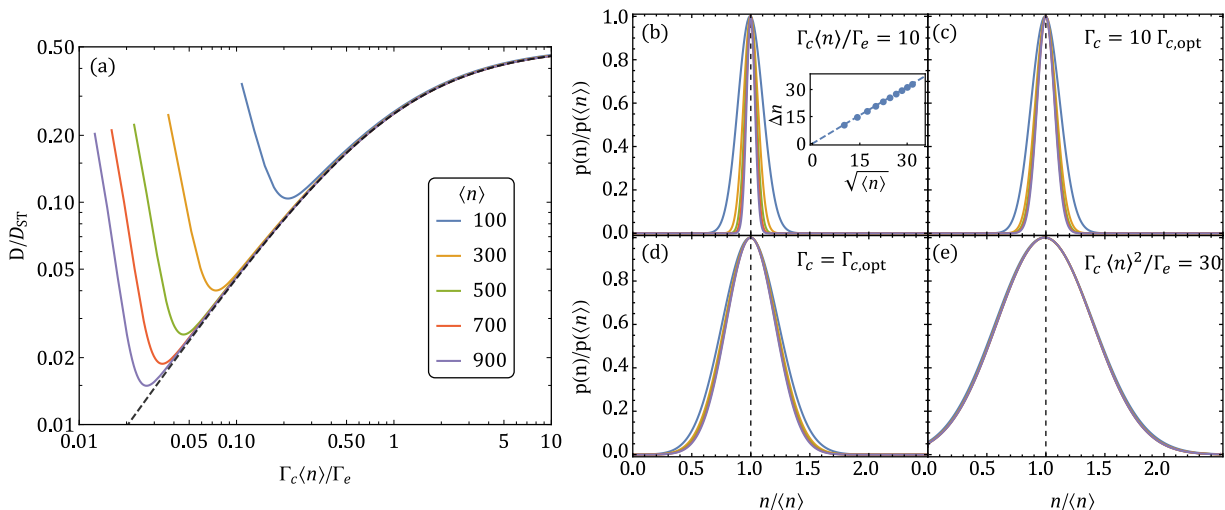


FIG. 3. The Susskind-Glogower Bare Operator (SGBO) laser. (a) Minimum laser linewidth can be achieved by tuning the ratio of power emitted by conventional ($\langle n \rangle \Gamma_c$) and bare operator (Γ_e) loss for different cavity occupancies. The dotted line represents Eq. (5). Photon number distributions are shown in (b-e) for four cases: conventional loss is very weak (b); minimum linewidth (c); intermediate conventional loss (d); and conventional loss is dominant (e).

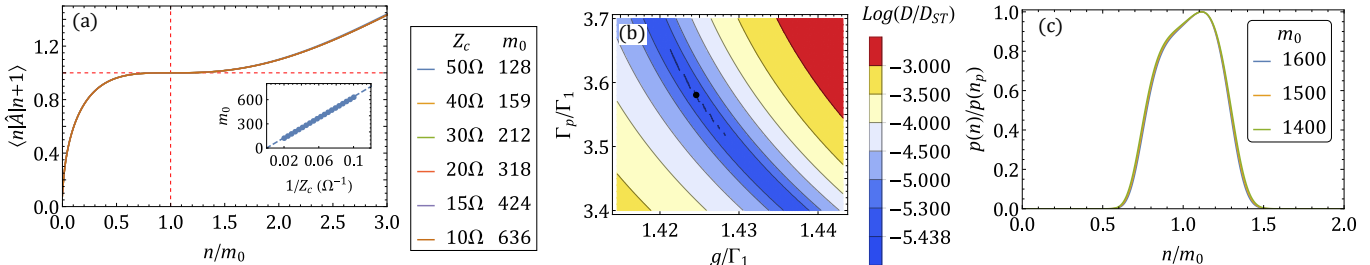


FIG. 4. Approximately Bare Operator Coupling Circuit (ABOCC) laser: (a) The matrix element $\langle n | \hat{A}_{c,m_0} | n+1 \rangle$ as a function of the photon number in the cavity show a plateau on which the matrix element is independent of the photon number thus approximating the bare operator. The matrix elements were computed for several values of the cavity impedance Z_c which controls m_0 as shown in the inset (the impedance of the qubit was set to $Z_a = 45.29 \Omega$). (b) Tuning the ABOCC laser by varying the pump power Γ_p and the atom-cavity coupling strength g that is controlled by $I_{J:a-c}$. (c) The photon number distributions of the optimum linewidth point at various m_0 values.

coupling

$$H_{a-c}^{(SGBO)} = g_2 (\hat{\sigma}^+ \hat{e}^- + \hat{\sigma}^- \hat{e}^+), \quad (3)$$

where e and e^\dagger are defined in Eq. (1). We extend Wiseman's scheme by setting the cavity loss super-operator to be

$$\hat{\mathcal{L}}_{c-tl}^{(SGBO)} = \Gamma_e \mathcal{D}[\hat{e}] + \Gamma_c \mathcal{D}[\hat{a}], \quad (4)$$

where Γ_e controls the rate of loss by the bare operators while Γ_c controls the rate of the conventional loss mechanism. This extension can be thought as a form of bath engineering. A small amount of conventional loss is essential for stabilizing the laser as, without it, neither the rate at which photons are pumped into the cavity, nor the rate at which photons leave the cavity depends on the number of photons in the cavity, and hence the laser becomes unstable.

We can achieve this tremendous reduction in linewidth as the bare operator couplings allow photons to enter and leave the laser cavity without inducing phase noise (and hence they do not directly contribute to the linewidth). On the other hand, the photon number operator is conjugate to the phase operator, and therefore in the presence of only bare operator couplings the distribution of photon numbers in the cavity becomes infinitely broad. Adding conventional loss makes the photon number distribution have finite width, thereby stabilizing the laser at the cost of introducing phase noise. While both the conventional and the bare operator loss are contributing to the laser luminosity, only the conventional loss is contributing to the laser linewidth, and therefore the ratio of the SGBO laser linewidth D_{SGBO} to the generalized Schawlow-Townes limit is

$$\frac{D_{SGBO}}{D_{ST}} = \frac{\langle n \rangle \Gamma_c}{2(\Gamma_e + \langle n \rangle \Gamma_c)}. \quad (5)$$

In Fig. 3a we plot the linewidth ratio $D_{\text{SGBO}}/D_{\text{ST}}$ as a function of $\Gamma_c\langle n\rangle/\Gamma_e$, the ratio between power emitted by conventional and bare operator loss while keeping the mean photon number fixed (see methods). We observe that as we decrease $\Gamma_c\langle n\rangle/\Gamma_e$, the ratio $D_{\text{SGBO}}/D_{\text{ST}}$ first follows Eq. (5), then saturates at a point that depends on the number of photons in the cavity, and then begins increasing again. The origin of saturation and increase can be understood by looking at the distribution of photon numbers in the laser cavity.

When $\Gamma_c\langle n\rangle/\Gamma_e$ is large, conventional loss dominates and the distribution of photon numbers in the cavity has a width $\sim \sqrt{\langle n\rangle}$ (Fig. 3b). As $\Gamma_c\langle n\rangle/\Gamma_e$ decreases, the distribution of photon numbers in the cavity broadens (Fig. 3c). This continues until the distribution width Δn becomes roughly half of $\langle n\rangle$, at which point the linewidth saturates and the photon distribution becomes universal (Fig. 3d). As $\Gamma_c\langle n\rangle/\Gamma_e$ is decreased even further, the photon number distribution becomes even broader (Fig. 3e) and the probability to have no photons in the cavity becomes appreciable. The state with no photons in the cavity does not have a well defined phase. Consequently, the occupation of this state dominates the broadening of the laser linewidth for small $\Gamma_c\langle n\rangle/\Gamma_e$.

We now take on the challenge of engineering the bare operators. We start with the atom-cavity coupling. The key property of the \hat{e} operator is that the matrix element $|\langle n-1|\hat{e}|n\rangle| = 1$ is independent of n , while for the standard photon annihilation operator \hat{c} , $|\langle n-1|\hat{c}|n\rangle| = n^{1/2}$. We have come up with the coupling circuit, depicted in Fig. 1, composed of an AC-SQUID (a Josephson junction shunted by a linear inductor) with an additional π junction to ground (the π junctions could be made from, for example, a second AC-SQUID that is flux-biased). The atom-cavity coupling induced by this circuit is described by the Hamiltonian

$$H_{\text{a-c}}^{\text{(ABOCC)}} = g \left(\hat{\sigma}^+ \hat{A}_{c,m_0} + \hat{\sigma}^- \hat{A}_{c,m_0}^\dagger \right), \quad (6)$$

where \hat{A}_{c,m_0} is an effective cavity photon annihilation operator and the atom-cavity coupling strength g is controlled by the critical current ($I_{\text{J:a-c}}$) of the Josephson junction in the ABOCC and the normalization parameter \mathcal{N} of the ABOCC cavity operator \hat{A}_{c,m_0} (see methods Eq. (9)). The operator \hat{A}_{c,m_0} is designed to work when there are m_0 photons in the laser cavity, where m_0 depends on the transmon and cavity impedances (see inset of Fig. 4a and methods). In Fig. 4a we plot the matrix element $\langle n|\hat{A}_{c,m_0}|n+1\rangle$ as a function of n/m_0 . We observe that the matrix element has a plateau, centered on $n = m_0$, around which it is independent of n . The plateau is obtained by combining the sinusoidal current phase relation of the Josephson junction with the linear current phase of the inductor in the coupling circuit (see methods). On this plateau, \hat{A}_{c,m_0} behaves approximately like the bare operator \hat{e} . We remark that the fact that in Fig. 4a the matrix element traces with different m_0 's

collapse indicates that the range of n 's over which \hat{A}_{c,m_0} behaves like \hat{e} also scales with m_0 .

Introducing an ABOCC to the cavity-transmission line coupling results in the cavity loss operator

$$\hat{\mathcal{L}}_{\text{c-tl}}^{\text{ABOCC}} = \Gamma_1 \mathcal{D}[\hat{B}_{c,m_0}], \quad (7)$$

where Γ_1 is the rate constant determined by the critical current of the Josephson junction of the coupling circuit, \hat{B}_{c,m_0} is similar to \hat{A}_{c,m_0} but takes into account properties of the transmission line (see methods and supplementary material).

The ABOCC laser, in which we use ABOCCs for both atom-cavity and cavity-transmission line couplings, is stable and does not require conventional loss like the SGBO laser. To tune up the ABOCC laser we first choose the desired number of photons in the cavity and then set the impedances of the inverted transmon qubit, the cavity and the transmission line so that both ABOCCs have the desired value of m_0 . Next, we vary the transmon qubit's inverting incoherent pump strength Γ_p (see [38, 39] and the online supplement for how to implement this drive) and the atom-cavity coupling strength g while fixing the cavity-transmission line coupling strength in order to minimize the ratio $D_{\text{ABOCC}}/D_{\text{ST}}$ (see Fig. 4b).

The general performance characteristics of the ABOCC laser are very similar to those of the SGBO laser. Both have a linewidth which is a factor of $1/\langle n\rangle$ narrower than the generalized Schawlow-Townes limit (see Fig. 2). At the optimal operating point, both have a photon distribution in the cavity with a width that scales with $\langle n\rangle$ as opposed to $\langle n\rangle^{1/2}$ for conventional lasers (see Fig. 3d and 4c). There is, however, a difference in the shape of the distributions. In the case of the SGBO laser the photon distribution width is limited by occupation of the empty state. On the other hand in the ABOCC laser it is limited by the width of the plateau on which the operator \hat{A}_{c,m_0} behaves like the bare operator (see Fig. 4a). However in both cases the limit scales with the photon number and hence the two lasers behave in similar ways.

Our results raise the question: given our demonstrated ability to greatly exceed the standard quantum limit, what is the 'ultimate' quantum limit on the linewidth of a laser? During the final stages of preparation of our manuscript we became aware of a pair of recent papers which argue that the ST limit divided by n^2 , which the authors call the Heisenberg limit, is the ultimate limit on laser linewidth [40, 41]. Our laser circuit already far exceeds the ST limit, operating at the geometric mean of the ST and the Heisenberg limit. However, there appears to still be some room for future improvements.

In summary, we have shown that by engineering the photon loss operator it is possible to build a laser that is $\langle n\rangle$ times narrower than the standard quantum limit, where $\langle n\rangle$ is the number of photons in the laser cavity. We have also developed a realistic roadmap for constructing this type of laser using standard circuit QED components: capacitors, inductors and Josephson junctions.

These are exactly the same components that are used in a wide variety of superconducting quantum information devices. The photon field in the cavity of the proposed laser is highly squeezed with the photon number distribution width scaling with the photon number (as opposed to the square-root of the photon number that is observed in conventional lasers). The proposed device can be thought of as approaching the Heisenberg limit on phase estimation. It is both an interesting source of quantum light for quantum information experiments, and shows how even well-understood quantum optical objects such as lasers can be re-imagined with the techniques of quantum information and the tools of superconducting circuits.

METHODS

To describe the lasers we use the master equation

$$\dot{\rho} = \hat{\mathcal{L}}_a[\rho] - \frac{i}{\hbar}[H_{a-c}, \rho] - \frac{i}{\hbar}[H_c, \rho] + \hat{\mathcal{L}}_{c-tl}[\rho]. \quad (8)$$

The Hamiltonian H_{a-c} describes that atom-cavity coupling and the super-operator $\hat{\mathcal{L}}_{c-tl}[\rho]$ describes loss of cavity photons to the transmission line. The super-operator $\hat{\mathcal{L}}_a[\rho] = -\frac{i\omega_a}{2}[\sigma^z, \rho] + \Gamma_p \mathcal{D}[\sigma^+]\rho$ describes the artificial atom, where σ^z is the atom Pauli matrix and $\mathcal{D}[\sigma^+]\rho = \sigma^+ \rho \sigma^- - \frac{1}{2}(\sigma^- \sigma^+ \rho + \rho \sigma^- \sigma^+)$ describes the action of the incoherent pump. The Hamiltonian $H_c = \omega_c c^\dagger c$ describes the cavity energy levels, where c is the photon annihilation operators in the cavity and we set $\omega_c = \omega_a$.

To obtain the linewidth of the laser we numerically find the eigenspectrum of the time evolution super-operator defined by the right hand side of Eq. (8). The eigenspectrum is non-positive, and is composed of a zero eigenvalue corresponding to the steady state of the laser and a number of negative eigenvalues. The largest of these negative eigenvalues (i.e. the smallest by magnitude) correspond to the laser linewidth.

To optimize the SGB0 laser (Fig. 3a): (1) We work in the strong atom-cavity coupling regime by fixing $g_2 = 1000\sqrt{\Gamma_p \Gamma_e}$. In this regime we estimate the mean photon number to be $\langle n \rangle \sim (\Gamma_p - 2\Gamma_e)/(2\Gamma_c)$. (2) We tune Γ_p/Γ_e and Γ_c/Γ_e to optimize the laser linewidth while fixing the mean number of photons in the cavity.

The ABOCC coupling the atom to the cavity is described by the Hamiltonian

$$H_{a-c}^{(ABOCC)} = \frac{\phi_0^2 \hat{\delta}^2}{2L_{a-c}} - E_{J:a-c} \cos \hat{\delta} + E_{J:c} \cos \hat{\phi}_c,$$

where $\hat{\delta} = \hat{\phi}_a - \hat{\phi}_c$ and $\hat{\phi}_a$ and $\hat{\phi}_c$ are the superconducting phase operators of the transmon and the cavity; $\phi_0 = \Phi_0/2\pi$; $E_{J:a-c} = \Phi_0 I_{J:a-c}$ and L_{a-c} are the Josephson energy and the linear inductance of the AC SQUID part of the ABOCC and $E_{J:c}$ is the Josephson energy of the π junction.

Expressing the phase operators in terms of creation and annihilation operators and applying the rotating wave approximation we obtain Eq. (6), where

$$\hat{A}_{c,m_0} = \frac{1}{\mathcal{N}} \left(\frac{\phi_0^2 \tilde{\phi}_a \tilde{\phi}_c c}{L_{a-c} E_{J:a-c}} - \sin(\tilde{\phi}_a) e^{-\frac{\tilde{\phi}_c^2}{2}} \sum_{n=0}^{\infty} \frac{(-1)^n \tilde{\phi}_c^{2n+1} (c^\dagger)^n c^{n+1}}{n!(n+1)!} \right). \quad (9)$$

and $\tilde{\phi}_{a,c} = \frac{1}{\phi_0} \sqrt{\frac{\hbar Z_{a,c}}{2}}$ and \mathcal{N} is a normalization factor that ensures that $\langle m_0 | A_{c,m_0} | m_0 + 1 \rangle = 1$.

Γ_1 and \hat{B}_{c,n_p} that appear in Eq. (7) are

$$\Gamma_1 = \mathcal{N} \frac{E_{J:c-tl}^2}{\hbar^2} \left(\frac{\hbar Z_{tl}}{2\phi_0^2} \right) \frac{1}{\omega_c} \quad (10)$$

$$\hat{B}_{c,m_0} = \frac{1}{\mathcal{N}} \left(\mathcal{C}_{TL} e^{-\tilde{\phi}_c^2/2} \sum_{n=0}^{\infty} \frac{(-1)^n \tilde{\phi}_c^{2n+1}}{n! \cdot (n+1)!} (c^\dagger)^n c^{n+1} + \frac{2\phi_0^2 \tilde{\phi}_c}{L_{c-tl} E_{J:c-tl}} c \right), \quad (11)$$

$\mathcal{C}_{TL} = \exp\left(-\frac{1}{\phi_0^2} \frac{\hbar Z_T}{4\pi}\right) \left[1 + \frac{\theta}{\omega_c} + \frac{\theta^2}{2\omega_c^2} + O\left(\frac{\theta^3}{\omega_c^3}\right)\right]$ and $\theta \ll \omega_c$ is the bandwidth of the transmission line.

ACKNOWLEDGMENTS

We thank Andrew Daley and John Jeffers for insightful comments. C. Liu acknowledges support from a Pittsburgh Quantum Institute graduate student fellowship. Research was also supported by the Army Research Office under Grants Number W911NF-18-1-0144 and W911NF-15-1-0397, and by M. Hatridge's NSF CAREER grant (PHY-1847025). G.D. was partially supported by NSF EFRI ACQUIRE 1741656. The views and conclusions contained in this document are those of the authors and should not be interpreted as representing the official policies, either expressed or implied, of the Army Research Office or the U.S. Government. The U. S. Government is authorized to reproduce and distribute reprints for Government purposes notwithstanding any copyright notation herein.

-
- [1] A. L. Schawlow and C. H. Townes, Phys. Rev. **112**, 1940 (1958).
 [2] L. Susskind and J. Glogower, Physics Physique Fizika **1**, 49 (1964).

- [3] S. Barnett, S. Stenholm, and D. Pegg, Optics Communications **73**, 314 (1989).
 [4] H. M. Wiseman, Phys. Rev. A **60**, 4083 (1999).

- [5] D. Gottesman, A. Kitaev, and J. Preskill, *Phys. Rev. A* **64**, 012310 (2001).
- [6] N. C. Menicucci, *Phys. Rev. Lett.* **112**, 120504 (2014).
- [7] K. Marshall, C. S. Jacobsen, C. Schäfermeier, T. Gehring, C. Weedbrook, and U. L. Andersen, *Nature Communications* **7**, 13795 (2016).
- [8] N. Didier, A. Kamal, W. D. Oliver, A. Blais, and A. A. Clerk, *Phys. Rev. Lett.* **115**, 093604 (2015).
- [9] A. Eddins, S. Schreppler, D. M. Toyli, L. S. Martin, S. Hacoen-Gourgy, L. C. G. Govia, H. Ribeiro, A. A. Clerk, and I. Siddiqi, *Phys. Rev. Lett.* **120**, 040505 (2018).
- [10] C. M. Caves, *Phys. Rev. D* **23**, 1693 (1981).
- [11] R. S. Bondurant and J. H. Shapiro, *Phys. Rev. D* **30**, 2548 (1984).
- [12] Y. Ma, H. Miao, B. H. Pang, M. Evans, C. Zhao, J. Harms, R. Schnabel, and Y. Chen, *Nature Physics* **13**, 776 (2017).
- [13] X. Zuo, Z. Yan, Y. Feng, J. Ma, X. Jia, C. Xie, and K. Peng, *Phys. Rev. Lett.* **124**, 173602 (2020).
- [14] H. Yuen and J. Shapiro, *IEEE Transactions on Information Theory* **24**, 657 (1978).
- [15] R. E. Slusher and B. Yurke, *Journal of Lightwave Technology* **8**, 466 (1990).
- [16] D. Gottesman and J. Preskill, “Secure quantum key distribution using squeezed states,” in *Quantum Information with Continuous Variables*, edited by S. L. Braunstein and A. K. Pati (Springer Netherlands, Dordrecht, 2003) pp. 317–356.
- [17] H. Vahlbruch, M. Mehmet, S. Chelkowski, B. Hage, A. Franzen, N. Lastzka, S. Gößler, K. Danzmann, and R. Schnabel, *Phys. Rev. Lett.* **100**, 033602 (2008).
- [18] S. Bartalini, S. Borri, P. Cancio, A. Castrillo, I. Galli, G. Giusfredi, D. Mazzotti, L. Gianfrani, and P. De Natale, *Phys. Rev. Lett.* **104**, 083904 (2010).
- [19] J. G. Bohnet, Z. Chen, J. M. Weiner, D. Meiser, M. J. Holland, and J. K. Thompson, *Nature* **484**, 78 (2012).
- [20] Y. Yamamoto, S. Machida, and O. Nilsson, *Phys. Rev. A* **34**, 4025 (1986).
- [21] H. Walther, B. T. Varcoe, B.-G. Englert, and T. Becker, *Reports on Progress in Physics* **69**, 1325 (2006).
- [22] S. M. Girvin, *Circuit QED: superconducting qubits coupled to microwave photons* (Oxford University Press, 2014).
- [23] V. E. Manucharyan, J. Koch, L. I. Glazman, and M. H. Devoret, *Science* **326**, 113 (2009).
- [24] J. Koch, T. M. Yu, J. Gambetta, A. A. Houck, D. I. Schuster, J. Majer, A. Blais, M. H. Devoret, S. M. Girvin, and R. J. Schoelkopf, *Phys. Rev. A* **76**, 042319 (2007).
- [25] J. A. Schreier, A. A. Houck, J. Koch, D. I. Schuster, B. R. Johnson, J. M. Chow, J. M. Gambetta, J. Majer, L. Frunzio, M. H. Devoret, S. M. Girvin, and R. J. Schoelkopf, *Phys. Rev. B* **77**, 180502 (2008).
- [26] A. A. Clerk, M. H. Devoret, S. M. Girvin, F. Marquardt, and R. J. Schoelkopf, *Rev. Mod. Phys.* **82**, 1155 (2010).
- [27] N. Bergeal, F. Schackert, M. Metcalfe, R. Vijay, V. Manucharyan, L. Frunzio, D. Prober, R. Schoelkopf, S. Girvin, and M. Devoret, *Nature* **465**, 64 (2010).
- [28] O. Astafiev, K. Inomata, A. O. Niskanen, T. Yamamoto, Y. A. Pashkin, Y. Nakamura, and J. S. Tsai, *Nature* **449**, 588 (2007).
- [29] F. Chen, J. Li, A. D. Armour, E. Brahim, J. Stettenheim, A. J. Sirois, R. W. Simmonds, M. P. Blencowe, and A. J. Rimberg, *Phys. Rev. B* **90**, 020506 (2014).
- [30] C. Rolland, A. Peugeot, S. Dambach, M. Westig, B. Kubala, Y. Mukharsky, C. Altimiras, H. le Sueur, P. Joyez, D. Vion, P. Roche, D. Esteve, J. Ankerhold, and F. Portier, *Phys. Rev. Lett.* **122**, 186804 (2019).
- [31] M. C. Cassidy, A. Bruno, S. Rubbert, M. Irfan, J. Kammhuber, R. N. Schouten, A. R. Akhmerov, and L. P. Kouwenhoven, *Science* **355**, 939 (2017).
- [32] S. H. Simon and N. R. Cooper, *Phys. Rev. Lett.* **121**, 027004 (2018).
- [33] D. K. L. Oi, V. Potoček, and J. Jeffers, *Phys. Rev. Lett.* **110**, 210504 (2013).
- [34] L. C. G. Govia, E. J. Pritchett, and F. K. Wilhelm, *New Journal of Physics* **16**, 045011 (2014).
- [35] S. Rosenblum, O. Bechler, I. Shomroni, Y. Lovsky, G. Guendelman, and B. Dayan, *Nature Photonics* **10**, 19 (2016).
- [36] M. Um, J. Zhang, D. Lv, Y. Lu, S. An, J.-N. Zhang, H. Nha, M. S. Kim, and K. Kim, *Nature Communications* **7**, 11410 (2016).
- [37] J. C. J. Radtke, D. K. L. Oi, and J. Jeffers, *Journal of Physics B: Atomic, Molecular and Optical Physics* **50**, 215501 (2017).
- [38] R. Ma, B. Saxberg, C. Owens, N. Leung, Y. Lu, J. Simon, and D. I. Schuster, *Nature* **570**, E52 (2019).
- [39] M. Mucci, X. Cao, C. Liu, R. Kaufman, D. Pekker, and M. Hatridge (APS, 2020).
- [40] H. M. Wiseman, S. N. Saadatmand, T. J. Baker, and D. W. Berry, in *Rochester Conference on Coherence and Quantum Optics (CQO-11)* (Optical Society of America, 2019) p. M3A.1.
- [41] T. J. Baker, S. N. Saadatmand, D. W. Berry, and H. M. Wiseman, “The heisenberg limit for laser coherence,” (2020), arXiv:2009.05296.
- [42] M. O. Scully and M. S. Zubairy, *Quantum Optics* (Cambridge University Press, 1997).
- [43] C. Gardiner, P. Zoller, and P. Zoller, *Quantum Noise: A Handbook of Markovian and Non-Markovian Quantum Stochastic Methods with Applications to Quantum Optics*, Springer Series in Synergetics (Springer, 2004).
- [44] H.-J. Briegel and B.-G. Englert, *Phys. Rev. A* **47**, 3311 (1993).
- [45] C. Ginzler, H.-J. Briegel, U. Martini, B.-G. Englert, and A. Schenzle, *Phys. Rev. A* **48**, 732 (1993).
- [46] H.-J. Briegel, B.-G. Englert, C. Ginzler, and A. Schenzle, *Phys. Rev. A* **49**, 5019 (1994).
- [47] Here there will be another factor of 2, which is because of the coupling to the left-propagating modes and the right-propagating modes.

Appendix A: Engineering an artificial atom with population inversion

In our main text, we used an incoherent drive to pump the transmon qubit from its ground state to the excited state. In this section we provide a specific design recipe for how to build such an incoherent pump.

Our goal is to build an effective three-level-atom (see Fig. 5a), where the transition between the ground state $|g\rangle$ and the second excited state $|f\rangle$ is coherently driven while the second excited state experiences a fast decay to the first excited state $|e\rangle$. If the decay process is sufficiently fast, as the population of the atom is driven to the state $|f\rangle$, it quickly relaxes to $|e\rangle$ and we achieve population inversion on the two lasing levels $|g\rangle$ and $|e\rangle$. However, the single-photon transition between $|g\rangle$ and $|f\rangle$ for a transmon qubit is forbidden by selection rule. Therefore, we propose coupling a SNAIL qubit to the transmon qubit to form a composite system (see Fig. 5b). The key feature of the SNAIL qubit is that it has third order nonlinearity that makes the $|g\rangle \rightarrow |f\rangle$ transition allowed.

The level structure of the two qubit system is shown in Fig. 5c. We use $|g_t\rangle$, $|e_t\rangle$ and $|f_t\rangle$ to represent the ground, first, and second excited states of the transmon qubit. For the SNAIL qubit we use $|0_s\rangle$, $|1_s\rangle$ and $|2_s\rangle$, etc., to represent the ground, first excited, second excited, etc. states.

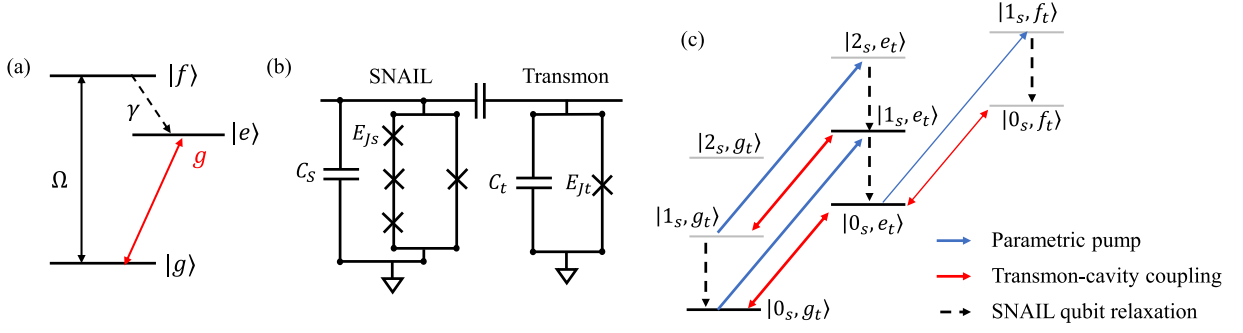


FIG. 5. In (a), we show the three-level model of the laser pump media (atom) where only coherent drives are permitted. In (b), we show the circuit diagram of the SNAIL qubit and transmon qubit composite system, in which the effective incoherent drive of the transmon qubit can be achieved. In (c) we show the level structure of the SNAIL qubit and the transmon qubit. The gray thin lines are the levels that are weakly populated in the pumping scheme discussed in Section A. The blue lines are the parametric drive on the composite system, the red arrows show the transition of the composite system due to the coupling to the laser cavity. The dashed arrows show the relaxation process of the SNAIL qubit. The thick solid lines show the transition that are on resonance, while the thin solid lines show the ones that are not on resonance (because of the anharmonicity of the transmon qubit).

Coupling of the SNAIL and transmon qubits results in the hybridization of their states. Consequently, third order non-linearity of the SNAIL qubit can be used to drive the $|0_s, g_t\rangle \rightarrow |1_s, e_t\rangle$ transition as the state $|1_s, e_t\rangle$ is hybridized with the state $|2_s, g_t\rangle$. This type of transitions are labeled by blue arrows in Fig. 5c. If the SNAIL qubit is also coupled to an output port, such that the relaxation of the SNAIL qubit [see Fig. 5c, black dashed arrows] is fast compared to the pump process (and also the transmon-cavity coupling, see Fig. 5c red arrows), then the two qubit system can form an effective three-level atom, in which $|0_s, g_t\rangle$ plays the role of the ground state ($|g\rangle$ in Fig. 5a), $|1_s, e_t\rangle$ the role of the second excited state ($|f\rangle$ in Fig. 5a), and $|0_s, e_t\rangle$ the role of the first excited state ($|e\rangle$ in Fig. 5(a)).

The Hamiltonian of a SNAIL qubit coupled to a transmon qubit is

$$H = H_T + H_S + H_{\text{couple}} \quad (\text{A1a})$$

$$H_T = \omega_t \hat{t}^\dagger \hat{t} + k_t \hat{t}^\dagger \hat{t}^\dagger \hat{t} \hat{t} \quad (\text{A1b})$$

$$H_S = \omega_s \hat{s}^\dagger \hat{s} + g_3 (\hat{s}^\dagger \hat{s}^\dagger \hat{s} + \hat{s}^\dagger \hat{s} \hat{s}) \quad (\text{A1c})$$

$$H_{\text{couple}} = g_2 (\hat{s}^\dagger \hat{t} + \hat{t}^\dagger \hat{s}) \quad (\text{A1d})$$

where \hat{s} (\hat{t}) is the photon annihilation operator for the SNAIL (transmon) qubit. We have also truncated the nonlinear parts of the Hamiltonians of both qubits to the lowest non-trivial order and dropped the rapidly rotating terms like $\hat{s}^\dagger \hat{s}^\dagger \hat{s}^\dagger$ and $\hat{s} \hat{s} \hat{s}$ in SNAIL qubit Hamiltonian. Finally, we make the assumption that the SNAIL and transmon qubits are strongly detuned as compared with the strength of the linear coupling, i.e., $2\Delta = |\omega_s - \omega_t| \gg g_2$, and hence the modes of the two qubits are only weakly hybridized. In the dressed basis, with respect to g_2 coupling, the third order nonlinearity of the bare SNAIL mode results in a third order nonlinear coupling between the dressed SNAIL and transmon modes $H_3 = \hat{s}^\dagger \hat{s}^\dagger \hat{t} + h.c.$, where \hat{s}' and \hat{t}' are the dressed SNAIL and transmon operators. Applying

parameter	variable	value
SNAIL qubit frequency	$\omega_s/(2\pi)$	7.2 GHz
SNAIL qubit 3rd order nonlinearity	$g/(2\pi)$	50 MHz
transmon qubit frequency	$\omega_t/(2\pi)$	6.7 GHz
transmon qubit 4th order nonlinearity	$k/(2\pi)$	-0.3 GHz
SNAIL-transmon coupling	$g_2/(2\pi)$	50 MHz
SNAIL coherent pump rate	$\Omega_d/(2\pi)$	2.0 GHz
SNAIL loss rate	$\gamma/(2\pi)$	5 MHz

TABLE I. Parameters used for numerical integration of Eq. A3 when generating figure Fig. 6

classical drive to the bare SNAIL mode

$$H_d = \Omega_d \exp[i(\omega_s + \omega_t)t] \hat{s} + h.c., \quad (\text{A2})$$

induces the two-photon pump process (see blue arrows in Fig. 5) via H_3 .

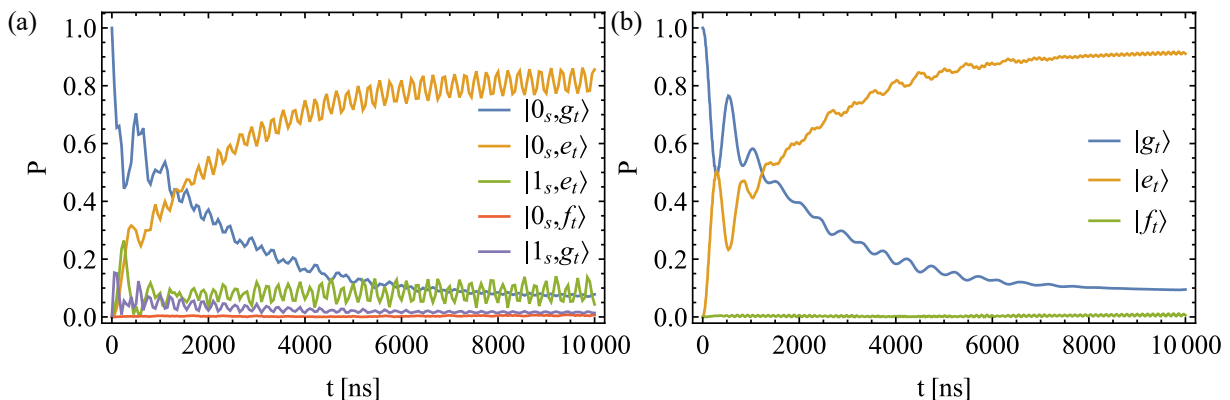


FIG. 6. Population inversion of the composite quantum system made up of a SNAIL and a transmon qubit under the influence of a coherent drive. (a) Population of the lowest five levels of the composite system (as labeled) plotted as a function of time. (b) Population of the transmon levels after tracing over the SNAIL qubit degrees of freedom. (See Table I for values of parameters used to construct this figure)

The composite quantum system can be described by the master equation

$$\partial_t \rho_{St} - i[H + H_d, \rho_{St}] + \gamma \mathcal{D}[\hat{s}] \rho_{St} \quad (\text{A3a})$$

$$\mathcal{D}[\hat{s}] \rho_{St} = -\frac{1}{2} (\hat{s}^\dagger \hat{s} \rho_{St} + \rho_{St} \hat{s}^\dagger \hat{s} - 2\hat{s} \rho_{St} \hat{s}^\dagger) \quad (\text{A3b})$$

where ρ_{St} is the density operator for the composite system of the coupled SNAIL and transmon qubits, the system Hamiltonian is given by Eq. (A1), and the classical drive Hamiltonian by Eq. (A2) and Eq. (A3b) describes the dissipation of the SNAIL mode.

To demonstrate that the proposed two-qubit system functions as a three level atom, we numerically integrate the the master equation, Eq. (A3). As the higher levels of the composite systems are weakly populated, we truncated the Hilbert space of the SNAIL qubit to allow a maximum of 6 photons, and the space of the transmon qubit to 3 photons. The populations of the lowest five states of the composite systems are shown in Fig. 6a. We observe that the coherent drive applied to the SNAIL qubit, together with the photon loss from the SNAIL qubit, induce an effectively population transfer from $|0_s, g_t\rangle$ to $|0_s, e_t\rangle$. We observe population inversion after $\sim 3\mu s$. At long times the system reaches a steady state with a significant population inversion (with roughly 90% occupancy of the state $|0_s, e_t\rangle$ and 10% of the state $|0_s, g_t\rangle$). The residual population of the state $|0_s, g_t\rangle$ is caused by the decay of the $|0_s, e_t\rangle$ via its hybridization with the state $|1_s, g_t\rangle$. The ripples on the population curves are caused by the classical drive on the SNAIL qubit which causes the SNAIL mode to have a fast oscillating component at the frequency $(\omega_s + \omega_t)$. In Fig. 6b, we plot the population of the ground, first and second excited states of the transmon qubit after tracing over the SNAIL qubit degrees of freedom. From this plot we observe that the transmon qubit is effectively being pumped from the ground state $|g_t\rangle$ to the first excited state $|e_t\rangle$. From the two plots in Fig. 6, we observe that the higher excited states of the composite systems (e.g., $|0_s, f_t\rangle$ and $|1_s, g_t\rangle$) have very little population, especially the second

excited state of the transmon qubit $|f_i\rangle$, which justifies the truncation of the composite system Hilbert space in our numerical calculation.

Appendix B: Describing the photon loss from the laser cavity to the transmission line induced by a linear inductive coupler

In this section we derive the effective photon loss operator for the laser cavity induced by a linear inductive coupling between the laser cavity (LC resonator) and the transmission line. We extend this description to the ABOCC in Sec. D.

The quantization of the LC resonator and the transmission line is discussed in Ref. [22, 26]. The canonical position and momentum of the LC resonator are the node superconducting phase φ_c and charge Q_c . Using these coordinates, the quadratic Hamiltonian of the LC resonator can be quantized, similar to the Harmonic oscillator, via

$$\hat{Q}_c = -i\sqrt{\frac{\hbar}{2Z_c}} (\hat{c} - \hat{c}^\dagger) \quad (\text{B1a})$$

$$\hat{\Phi}_c = \sqrt{\frac{\hbar Z_c}{2}} (\hat{c} + \hat{c}^\dagger) \quad (\text{B1b})$$

where Z_c is the characteristic impedance of the LC resonator, $Z_c = \sqrt{L_c/C_c}$, and the Hamiltonian of the LC resonator, in second quantized form, is $H_c = \hbar\omega_c \hat{a}^\dagger \hat{a}$, where the frequency of the LC resonator is $\omega_c = 1/\sqrt{L_c C_c}$. The voltage on the LC resonator is $V_c = \dot{\Phi}_c$ and the current flow in the LC resonator is $I_c = \dot{Q}_c$. We can express the voltage and current operators using the raising and lowering operators via

$$\hat{V}_c = -\frac{i}{\hbar} [\hat{\Phi}_c, H_c] = -i\omega \sqrt{\frac{\hbar Z_c}{2}} (\hat{c} - \hat{c}^\dagger), \quad (\text{B2a})$$

$$\hat{I}_c = -\frac{i}{\hbar} [\hat{Q}_c, H_c] = \omega \sqrt{\frac{\hbar}{2Z_c}} (\hat{c} + \hat{c}^\dagger). \quad (\text{B2b})$$

Here we consider a single-mode transmission line that couples to the LC resonator via a linear inductor. The generalized flux along the transmission line is

$$\Phi(x, t) = \int_{-\infty}^t d\tau V(x, \tau) = \frac{1}{\phi_0} \phi(x, t), \quad (\text{B3})$$

and the charge density along the transmission line $q(x)$ can be quantized. After the quantization of the transmission line fields, $\phi(x)$ and $q(x)$ are

$$\hat{q}(x) = \sum_{k=-\infty}^{+\infty} \sqrt{\frac{\hbar\omega_k C}{2l}} (\hat{b}_k e^{ikx} + \hat{b}_k^\dagger e^{-ikx}) \quad (\text{B4a})$$

$$\hat{\phi}(x) = -i \sum_{k=-\infty}^{+\infty} \sqrt{\frac{\hbar Z_T v_p}{2l\omega_k}} (\hat{b}_k e^{ikx} - \hat{b}_k^\dagger e^{-ikx}) \quad (\text{B4b})$$

where $v_p = 1/\sqrt{LC}$ is the wave speed along the transmission line and the dispersion relation of the mode with momentum k is $\omega_k^2 = v_p^2 k^2$, $Z_T = \sqrt{L/C}$ is the characteristic impedance of the transmission line, l is the total length of the transmission line.

We further assume that the linear inductive coupling element (L_{c-tl}) that couples the LC resonator and the transmission line, connects to the $x = 0$ point of the transmission line. The coupling Hamiltonian is given in Eq. (7) of the main text, where the dimensionless parameters $\tilde{\varphi}_c$ and $\tilde{\varphi}_T(k)$ are defined as

$$\tilde{\varphi}_c = \frac{1}{\phi_0} \sqrt{\frac{\hbar Z_c}{2}}, \quad \tilde{\varphi}_T(k) = \frac{1}{\phi_0} \sqrt{\frac{\hbar Z_T}{2}} \sqrt{\frac{v_p}{l\omega_k}}. \quad (\text{B5})$$

Here we only consider the LC resonator and the transmission line parts of the Josephson micromaser to understand the dissipation induced on LC resonator by the transmission line. The Hamiltonian of the system under consideration is

$$H = H_c + H_{tl} + H_{c-tl} = \hbar\omega_c \hat{c}^\dagger \hat{c} + \hbar \sum_k \omega_k \hat{b}_k^\dagger \hat{b}_k + i\hbar \sum_k \kappa_k (\hat{c}^\dagger \hat{b}_k - \hat{b}_k^\dagger \hat{c}), \quad (\text{B6})$$

where $\kappa_k = \frac{\phi_0^2}{\hbar L_{c-tl}} \tilde{\varphi}_c \varphi_{tl}(k)$. We further treat the transmission line as a vacuum bath, and apply the Born-Markov approximation to simplify the dynamics of the cavity field as in Ref. [42, Chap. 8]. The dynamics of the LC resonator mode can be described by the master equation

$$\partial_t \rho(t) = -\frac{i}{\hbar} [H_c, \rho(t)] - \frac{\gamma}{2} (\hat{c}^\dagger \hat{c} \rho(t) + \rho(t) \hat{c}^\dagger \hat{c} - 2\hat{c} \rho(t) \hat{c}^\dagger), \quad (\text{B7})$$

where ρ is the density operator for the LC resonator, and the decay rate

$$\gamma = \frac{Z_c Z_T}{2L_{c-tl} \omega_c}. \quad (\text{B8})$$

Appendix C: Obtaining the laser line shape and linewidth using the spectrum of the time-evolution super-operator

The phase noise of the laser cavity field causes the phase of the laser light to fluctuate, which gives a finite linewidth to the laser. Before proceeding with a detailed analysis, we begin by summarizing the key points. The master equation Eq. (C3) can be thought of as an eigenvalue problem Eq. (C7). The spectrum of eigenvalues has one zero eigenvalue $\lambda_0 = 0$, which corresponds to the steady state solution of the laser, and a number of negative eigenvalues $\lambda_{i \neq 0} < 0$ which correspond to the decaying modes. As we show in this section, the spectral representation of the two-time correlation function $G(t + \tau, t)$ that describes the decay of coherence consists of a linear combination of decaying exponentials with the decay time set by these negative eigenvalues, see Eq. (C10). To obtain the laser line shape we go to Fourier space. In the Fourier representation, $G(\omega)$ consists of a linear combination of Lorentzians with width set by the negative eigenvalues. Moreover, almost all of the weight ($\sim 97.32\%$ for the ABOCC laser example in this section) is carried by the Lorentzian with the largest nonzero eigenvalue (that is narrowest of the Lorentzians). It is precisely this Lorentzian that forms the central peak of the laser line shape, while the remaining Lorentzians contribute to slightly broadening the ‘‘pedestal’’ at the base of the central peak, see Fig. 7.

For a conventional laser system phase noise results in the two-time correlation function decaying as [42]

$$G(t + \tau, t) = \langle a^\dagger(t + \tau) a(t) \rangle \sim \langle n \rangle \exp(-i\omega_c \tau - D\tau). \quad (\text{C1})$$

The power spectrum of the laser is given by the Fourier transform of the two-time correlation function $G(t + \tau, t)$,

$$S(\omega) = \frac{1}{\pi} \text{Re} \int \langle a^\dagger(t + \tau) a(t) \rangle e^{i\omega \tau} d\tau = \frac{\langle n \rangle}{\pi} \frac{D}{(\omega - \omega_c)^2 + D^2}, \quad (\text{C2})$$

which is a Lorentzian with full-width at half minimum $2D$, where D is the linewidth of the laser field.

For a system that couples to a Markovian bath, which can be described by the master equation

$$\partial_t \rho(t) = \hat{\mathcal{L}} \rho(t) \quad (\text{C3})$$

where $\hat{\mathcal{L}}$ is the super-operator acting on the system density operator (ρ), the time-evolution of the density operator can be formally solved by

$$\rho(t) = V(t, t_0) \rho(t_0) = e^{\hat{\mathcal{L}}(t-t_0)} \rho(t_0) \quad (\text{C4})$$

where $V(t, t_0)$ is a time-evolution super-operator that acts on the system degrees of freedom and $\rho(t_0)$ is the initial state of the laser system [43]. Also notice that the two-time correlator can be obtained via

$$G(t + \tau, t) = \text{Tr}_{S+B} [U^\dagger(t + \tau) a^\dagger U(t + \tau) U^\dagger(t) a U(t) R_0] = \text{Tr}_S \{ a^\dagger \text{Tr}_B [U(\tau) a R(t) U^\dagger(\tau)] \}, \quad (\text{C5})$$

where U is the time-evolution operator for the system and the bath, R is the density operator for both the system and the bath and Tr_S , Tr_B , Tr_{S+B} are trace over system, bath, system and bath degrees of freedom, respectively. The term $\text{Tr}_B [U(\tau) a R(t) U^\dagger(\tau)]$ can be thought of as a time-evolution of the ‘‘state’’ $aR(t)$ by a time period τ , which is $\{V(\tau, 0)[a\rho(t)]\}$ according to Eq. (C4). For the laser system, we are only interested in the laser linewidth when the system is stable, i.e., $\text{Tr}_S (a^\dagger(\tau) a \rho_s)$, where ρ_s is the steady state of the system, then the two-time correlation function can be written as

$$G(\tau) = \text{Tr}_S [a^\dagger e^{\hat{\mathcal{L}}\tau} (a \rho_s)] \quad (\text{C6})$$

Similar to the time-evolution of a closed quantum system, where we study the eigenstates of the Hamiltonian operator to understand the system dynamics, we can also find the eigen-spectrum of super-operator $\hat{\mathcal{L}}$ (so called damping basis) to study the time-evolution of the open quantum systems whose dynamics is described by the master equation Eq. (C3) [44–46]. The right-eigenstates of the super-operator $\hat{\mathcal{L}}$ can be defined as

$$\hat{\mathcal{L}}\hat{u}^{(i)} = \lambda^{(i)}\hat{u}^{(i)} \quad (\text{C7})$$

where λ_i is the corresponding eigenvalue. Notice that for any physical systems, the steady states are invariant under the time evolution, which means they are the nullspace of the super-operators. These states should be valid quantum states, i.e., they should have unit trace. Further, because the master equation should preserve the trace of the density operator, all the eigenstates with nonzero eigenvalues should have zero trace.

Suppose $a\rho_s$ in Eq. (C6) can be expanded using the the right eigenstates as

$$a\rho_s = c_0\hat{u}^{(0)} + \sum_i c_i\hat{u}^{(i)} \quad (\text{C8})$$

where c 's are the corresponding expansion coefficients and $c_0\hat{u}^{(0)}$ corresponding to the steady state solution, the two-time correlation function can be calculated as,

$$G(\tau) = c_0\text{Tr}_S [a^\dagger\hat{u}^{(i)}] + \sum_i c_i e^{\lambda^{(i)}\tau} \text{Tr}_S [a^\dagger\hat{u}^{(i)}] \quad (\text{C9})$$

$$= \sum_i c_i e^{\lambda^{(i)}\tau} \text{Tr}_S [a^\dagger\hat{u}^{(i)}] \quad (\text{C10})$$

where we take the fact that the density operator for steady state of a typical laser system is purely diagonal in the Fock basis, which kills the first term. Within all the right eigenstates of the super-operator $\hat{\mathcal{L}}$ which have significant contribution to the decay of the two-time correlation function ($c_i\text{Tr}_S[a^\dagger\hat{u}^{(i)}]$ term is large), the largest eigenvalue ($\hat{\mathcal{L}}$ is non-positive) contribute to the long-time performance, i.e., it controls the linewidth of the laser system.

To decompose the operator using the eigenstates of the super-operator $\hat{\mathcal{L}}$, notice that the super-operator is, in general, not Hermitian, the left eigenstates are needed to define the orthogonality relation. Following Ref. [44], the dual operator of the super-operator is defined as

$$\text{Tr}[A\hat{\mathcal{L}}(B)] = \text{Tr}[\check{L}(A)B] \quad (\text{C11})$$

for any operator A and state B . Then the left-eigenstates of the super-operator $\hat{\mathcal{L}}$ is

$$\check{v}^{(i)}\hat{\mathcal{L}} = \check{L}\check{v}^{(i)} = \lambda^{(i)}\check{v}^{(i)} \quad (\text{C12})$$

with orthonormal relation $\text{Tr}(\check{v}^{(i)}\hat{u}^{(j)}) = \delta_{i,j}$.

To numerically solve the eigenstates of the super-operator $\hat{\mathcal{L}}$, we notice in typical laser systems, the super-operator contains terms in the form of

$$\hat{\mathcal{L}}\rho = \sum_i \hat{\mathcal{L}}^{(i)}\rho = \sum_i \hat{P}^{(i)}\rho\hat{Q}^{(i)} \quad (\text{C13})$$

where $\hat{P}^{(i)}$ and $\hat{Q}^{(i)}$ operate on the system Hilbert space. After expanding the operators $\hat{P}^{(i)}$ and $\hat{Q}^{(i)}$ using a suitable basis of the system Hilbert space and acting on the system density operator, in the matrix form we get

$$\rho_{j,k}^{(i)} = \left(\hat{\mathcal{L}}^{(i)}\rho\right)_{j,k} = \sum_{l,m} \hat{P}_{j,l}^{(i)}\rho_{l,m}\hat{Q}_{m,k}^{(i)}, \quad (\text{C14})$$

where $\rho^{(i)} \equiv \hat{P}^{(i)}\rho\hat{Q}^{(i)}$. We can redefine the density operator as a vector, and hence the super-operator becomes a matrix, whose eigenvectors can be easily solved. To explicitly show the matrix representation of the master equation, we re-group the indices as

$$\rho_{j,k}^{(i)} = \left(\hat{\mathcal{L}}^{(i)}\rho\right)_{j,k} \rightarrow \rho_{jk}^{(i)} = \sum_{lm} \hat{\mathcal{L}}_{jk;lm}^{(i)}\rho_{lm} = \sum_{lm} \hat{P}_{j,l}^{(i)}\hat{Q}_{m,k}^{(i)}\rho_{lm} \quad (\text{C15})$$

and the super-operator becomes

$$\hat{\mathcal{L}} \rightarrow \hat{\mathcal{L}}_{jk;lm} = \sum_i \hat{P}_{j,l}^{(i)}\hat{Q}_{m,k}^{(i)}. \quad (\text{C16})$$

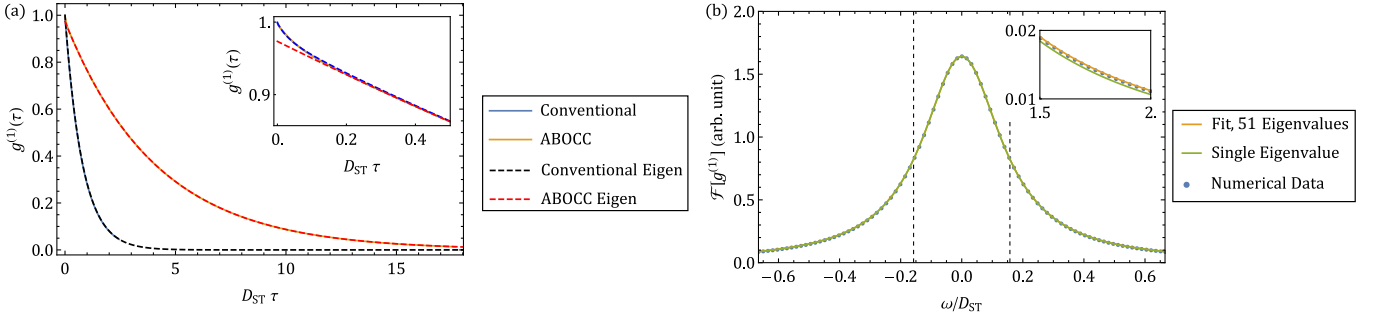


FIG. 7. In (a), we show the comparison between the numerical calculated two-time correlation function $g^{(1)}(\tau)$ versus the first eigenvalue of the laser systems. The numerical calculation is shown as solid lines (blue for conventional laser and orange for ABOCC laser), while the dashed lines are the exponential decay with the decay rate calculated by the eigen-spectrum of the super-operator. In the inset of (a), we zoom in on the ABOCC laser $g^{(1)}$ for short time period. The blue dashed line is the fitted decay of $g^{(1)}$ using the first 51 nonzero eigenvalues of the ABOCC laser system. In (b), we show the Fourier transform of the $g^{(1)}$ function. The fitted $g^{(1)}$ decay (orange line) matches with the numerical time evolution result (blue dots) well. The result using only the first nonzero eigenvalue is shown as the green line. Parameters: for conventional laser, $\Gamma_p = 30$, $\Gamma_c = 0.1$ and $g \sim 1.013$; for ABOCC laser: $m_0 = 43$ ($Z_c = 150 \Omega$), $\Gamma_1 = 1.0$, $\Gamma_p = 3.58$ and $g = 0.8747$.

The left and right eigenvectors of the matrix representation of the super-operator $\hat{\mathcal{L}}$ can be re-mapped back to the original index convention to get back the matrix representation in the system Hilbert space. The vector product of left and right eigen-vectors are equivalent to the product definition of the operators, i.e., the trace of the two operator product.

When we consider the laser system, especially we consider the cavity field, the Hilbert space is infinite dimensional. We can truncate the Hilbert space of the cavity field, but, in practice, the dimension is still very large and hence it is not practical to find all the eigenvectors of the super-operator. However, we notice that the right eigenvector with the lowest nonzero $|\lambda^{(i)}|$ is very close to $a\rho_s$. The other eigenstates, with larger $|\lambda^{(i)}|$, decay faster than this eigenstate and do not contribute significantly to the linewidth of the laser.

In Fig. 7a, we compare the numerical calculated normalized two-time correlation function $g^{(\tau)} = G(\tau)/\langle n \rangle$ using direct time-evolution of the master equations versus the function $d_1 e^{\lambda^{(1)}\tau}$ where d_1 is a coefficient that we fit and $\lambda^{(1)}$ is the largest nonzero eigenvalue of the super-operator $\hat{\mathcal{L}}$. In both the conventional laser system and ABOCC laser system, the decay of the normalized two-time correlation function from the numerical time-evolution method (solid lines) match well with the super-operator eigenvalues (dashed lines). For the ABOCC laser system, we also notice that at the small time-scale, the decay of the two-time correlation function slightly differs from the single eigenvalue fit (see the inset of Fig. 7a). This is caused by the finite overlapping to the other eigenstates which is responsible for the rapid initial decay. We fit the numerical time-evolved $g^{(1)}(\tau)$ function using first 20 eigenvalues (decay rates) of the super-operator of the ABOCC laser (blue dashed line), which gives a good fit to the direct time-evolution curve. From the fitting, we extract the overlap constant for the first nonzero eigenvalue of the super-operator is 0.9732, which means the main contribution of the long-time decay is given by the eigenstates with the largest nonzero eigenvalue. In Fig. 7b, we further examine the contribution to the linewidth in frequency domain. We Fourier transform the $g^{(1)}(\tau)$ data from both time-evolved method (blue dots) and the eigen-spectrum method (orange and green curves). We notice that the Fourier transform of fitted $g^{(1)}(\tau)$ using first 51 eigenvalues of the super-operator (the orange line) gives good agreement with the time-evolve method (blue dots). If we just extract the lineshape from the first eigenvalue (Fig. 7b green curve), the lineshape is slightly different from the time-evolution result (see inset). The difference is due to the finite overlap with the eigenstates that have a larger decay constant. However, the faster decaying states only contribute to the short-time dynamics (see Fig. 7a inset), which gives a slightly larger background on the Lorentzian lineshape and slightly increase the linewidth. However, the central peak of the spectrum is dominated by the first nonzero eigenvalue. In Fig. 7b, we observe that the Lorentzian based on the first nonzero eigenvalue (green curve) and the fitted time-evolution using the first 51 eigenvalues, and the numerically calculated lineshape all match well.

Compared to direct time-evolution method of calculating the laser dynamics, especially the steady state photon distribution and the laser linewidth or two-time correlation function, the eigen-spectrum method is significantly more computationally efficient. To further improve computational efficiency, we truncate the density matrices to include only the main diagonal and the first few minor diagonals. We verify that this truncation does not affect the part of the eigenspectrum that we are interested in by increasing the number of minor diagonals until convergence to the exact solution is reached for all values of $\langle n \rangle \leq 1000$ for the conventional and SGBO laser and $m_0 \leq 1000$ for the ABOCC laser.

Appendix D: Laser cavity loss with approximately bare operator coupling circuit (ABOCC)

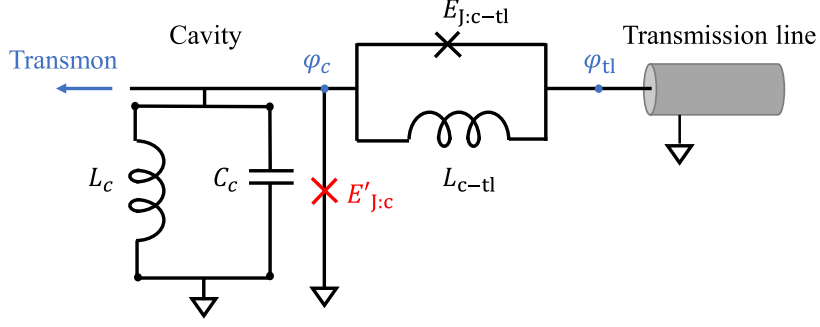


FIG. 8. The circuit diagram of the ABOCC coupling circuit between the cavity and the transmission line.

In our main text, the ABOCC coupling circuit between the cavity and the transmission line is shown in Fig. 1. The Hamiltonian for the ABOCC coupling is

$$H = -E_{J:c-tl} \cos(\hat{\varphi}_c - \hat{\varphi}_{tl}) + \frac{\phi_0^2}{2L_{c-tl}} (\hat{\varphi}_c - \hat{\varphi}_{tl})^2 + E'_{J:c} \cos(\hat{\varphi}_c), \quad (D1)$$

where $E_{J:c-tl}$ is the coupling Josephson junction energy, L_{c-tl} is the coupling linear inductance, $E'_{J:c}$ is the π -junction Josephson energy, and the node phase operators are $\hat{\varphi}_c$ and $\hat{\varphi}_{tl}$ as labeled in Fig. 8. The π -junctions are used to correct the dispersion given by the nonlinear coupling between the cavity and the transmission line. Here, we will ignore these two π junctions at the beginning of the discussion. Further, we define a dimensionless parameter $r = \frac{\phi_0^2}{2L_{c-tl}}/E_{J:c-tl}$. With the second quantization of the transmission line field and the LC resonator mode (see Section B of the online supplement), the phase across the ABOCC circuit is

$$\Delta\hat{\varphi} \equiv \hat{\varphi}_c - \hat{\varphi}_{tl} = \tilde{\varphi}_c (\hat{c} + \hat{c}^\dagger) + i \sum_k \tilde{\varphi}_{tl}(k) (\hat{b}_k - \hat{b}_k^\dagger). \quad (D2)$$

The coupling Hamiltonian (without the π junctions) becomes

$$H/E_{J:c-tl} = -\cos(\Delta\hat{\varphi}) + r\Delta\hat{\varphi}^2 = \frac{1}{2} (e^{i\hat{\varphi}_c} e^{-i\hat{\varphi}_{tl}} + e^{-i\hat{\varphi}_c} e^{i\hat{\varphi}_{tl}}) + \Delta\hat{\varphi}^2, \quad (D3)$$

where we have used the fact that the resonator operators and the transmission line field operators commute. We use the Baker-Campbell-Hausdorff formula to transform the exponential of the operators

$$e^{\pm i\hat{\varphi}_c} = e^{-\tilde{\varphi}_c^2/2} e^{\pm i\tilde{\varphi}_c \hat{c}^\dagger} e^{\pm i\tilde{\varphi}_c \hat{c}}, \quad e^{\pm i\hat{\varphi}_{tl}(k)} = e^{-\tilde{\varphi}_{tl}^2(k)/2} e^{\mp \tilde{\varphi}_{tl} \hat{b}_k^\dagger} e^{\pm \tilde{\varphi}_{tl} \hat{b}_k}. \quad (D4)$$

We will use this result in order to reach a normal ordering in which the LC resonator operators are to the right of the transmission line operators.

The expansion of Eq. (D3) to third order in the transmission line field operators yields

$$H/E_{J:c-tl} = h_c + h_{tl} + h_1 + h_2 + h_3 + \dots \quad (D5)$$

where h_c and h_{tl} are the dimensionless Hamiltonian acting solely on the cavity field and the transmission line, respectively. The cavity-transmission line coupling is expanded in orders of the transmission line field operators and the first, second and third order terms are labeled as h_1 , h_2 and h_3 .

$$h_c = - \left(\prod_k e^{-\tilde{\varphi}_{tl}^2(k)/2} \right) \frac{1}{2} (e^{i\hat{\varphi}_c} + e^{-i\hat{\varphi}_c}) + r\hat{\varphi}_c^2 \equiv -\mathcal{C}_{tl} \cos(\hat{\varphi}_c) + r\hat{\varphi}_c^2, \quad (D6a)$$

$$h_{tl} = -e^{-\tilde{\varphi}_c^2/2} \frac{1}{2} (e^{i\hat{\varphi}_{tl}} + e^{-i\hat{\varphi}_{tl}}) + r\hat{\varphi}_{tl}^2 \equiv -\mathcal{C}_c \cos(\hat{\varphi}_{tl}) + r\hat{\varphi}_{tl}^2, \quad (D6b)$$

where, \mathcal{C}_{TL} and \mathcal{C}_c are two constants. Notice that h_{sys} and h_{tl} , induced by the coupling circuit, contributes new nonlinearities to the cavity and the transmission line. These nonlinearities, especially the nonlinearity of the cavity

field, will degrade the laser performance by shifting the cavity frequency as the number of photons in the cavity increases. To compensate for these dispersive effects on the cavity, we include a π junction as shown in Fig. 8, in which the Josephson energies satisfy

$$E'_{J:c} = C_{tl}E_{J:c-tl}, \quad E'_{J:tl} = C_cE_{J:c-tl}. \quad (D7)$$

This π junctions cancel out the non-linear contributions of h_{tl} thus reducing dephasing. In the following discussion we focus on the remaining terms, which are the cavity-transmission line coupling terms h_1 , h_2 and h_3 .

Expansion of Eq. (D4) yields

$$h_1 = -iC_{TL} \sum_k \tilde{\varphi}_T(k)(b_k^\dagger - b_k) \sin(\hat{\varphi}_c) + 2ir\hat{\varphi}_c \sum_k \tilde{\varphi}_T(k) (b_k - b_k^\dagger), \quad (D8a)$$

$$h_2 = -C_{TL} \left\{ \sum_k \frac{\tilde{\varphi}_T^2(k)}{2} (b_k^2 + (b_k^\dagger)^2 - b_k^\dagger b_k) + \sum'_{k,q} \tilde{\varphi}_T(k)\tilde{\varphi}_T(q) (b_k b_q + b_k^\dagger b_q^\dagger - 2b_k^\dagger b_q) \right\} [\cos(\hat{\varphi}_c) - 1], \quad (D8b)$$

$$h_3 = -iC_{TL} \left\{ \sum_k \frac{\tilde{\varphi}_T^3(k)}{6} \left[(b_k^\dagger)^3 - 3(b_k^\dagger)^2 b_k + 3b_k^\dagger b_k^2 - b_k^3 \right] + \sum'_{k,q} \frac{\tilde{\varphi}_T^2(k)\tilde{\varphi}_T(q)}{2} \left[(b_k^\dagger)^2 + b_k^2 - 2b_k^\dagger b_k \right] (b_q^\dagger - b_q) \right. \\ \left. + \sum'_{k,q,p} \tilde{\varphi}_T(k)\tilde{\varphi}_T(q)\tilde{\varphi}_T(p) (b_k^\dagger - b_k) (b_q^\dagger - b_q) (b_p^\dagger - b_p) \right\} \sin(\hat{\varphi}_c), \quad (D8c)$$

where the summation \sum_k is from $-\infty$ to $+\infty$, the summations with prime $\sum'_{k,q}$ and $\sum'_{k,q,p}$ omit the terms in which any of the summation indices are equal.

We further assume that the coupling strength between the LC resonator and the transmission line, which is controlled by $E_{J:c-tl}$, is small compared to the LC resonator mode frequency and the transmission line dynamics, which allows us to apply the rotating-wave approximation (RWA). Applying the rotating wave approximation to h_1 of Eq. (D8a), and restoring dimensions of energy, we obtain

$$H_1 = -iE_J C_{TL} e^{-\hat{\varphi}_c^2/2} \sum_k \sum_{n=0}^{\infty} (-1)^n \frac{\tilde{\varphi}_T(k)\tilde{\varphi}_c^{2n+1}}{n! \cdot (n+1)!} \left[b_k^\dagger (a^\dagger)^n a^{n+1} - b_k (a^\dagger)^{n+1} a^n \right] \\ + 2irE_J \hat{\varphi}_c \sum_k \tilde{\varphi}_T(k) (a^\dagger b_k - b_k^\dagger a). \quad (D9)$$

Defining the nonlinear operator for the cavity field

$$\hat{A}_1 = C_{tl} e^{-\hat{\varphi}_c^2/2} \sum_{n=0}^{\infty} (-1)^n \frac{\tilde{\varphi}_c^{2n+1}}{n! \cdot (n+1)!} (a^\dagger)^n a^{n+1} + 2r\tilde{\varphi}_c a, \quad (D10)$$

and applying the Born-Markov approximation to trace over the transmission line degrees of freedom, the first order coupling contributes to a resonator dissipator term

$$\Gamma_1 \mathcal{D}[\hat{A}_1] \rho = -\frac{\Gamma_1}{2} \left(\hat{A}_1^\dagger \hat{A}_1 \rho + \rho \hat{A}_1^\dagger \hat{A}_1 - 2\hat{A}_1 \rho \hat{A}_1^\dagger \right), \quad (D11)$$

where the decay rate is

$$\Gamma_1 = \frac{E_J^2}{\hbar^2} \left(\frac{\hbar Z_T}{2\phi_0^2} \right) \frac{1}{\omega_c}. \quad (D12)$$

Before we move to the higher order nonlinear terms in the ABOCC Hamiltonian, we calculate the constant parameter C_{TL} , which is given by Eq. (D6). In the quantum optics regime, we assume that the transmission line has a large length, where we can assume $l \rightarrow \infty$. In this limit, we can approximate the summation of k by the integral of k as

$$\sum_k \rightarrow \frac{1}{2\pi} \int dk. \quad (D13)$$

Further, in quantum optics regime, especially for the system that Born-Markov approximation applies, the cavity frequency is the dominant frequency to the coupling bandwidth θ and the system-bath coupling strength. Here we explicitly assume that the cutoff frequencies for the system-bath coupling are $\omega_L = \omega_c - \theta/2$ and $\omega_H = \omega_c + \theta/2$, while the corresponding cutoff wave-vectors are k_L and k_H [47]. The constant \mathcal{C}_{TL} can be calculated as

$$\begin{aligned} \mathcal{C}_{\text{TL}} &= \prod_k e^{-\frac{\tilde{\varphi}_T(k)}{2}} = \exp \left[-\frac{1}{2} \sum_{k=k_L}^{k_H} \left(\frac{1}{\phi_0^2} \frac{\hbar Z_T}{2} \right) \frac{1}{kl} \right] \\ &\rightarrow \exp \left[-2 \frac{1}{4\pi} \left(\frac{1}{\phi_0^2} \frac{\hbar Z_T}{2} \right) \int_{k_L}^{k_H} \frac{1}{k} dk \right] \\ &= \exp \left(-\frac{1}{\phi_0^2} \frac{\hbar Z_T}{4\pi} \right) \frac{\omega_H}{\omega_L}, \end{aligned} \quad (\text{D14})$$

where ω_H and ω_L are the high and low frequencies of the bandwidth. Next, we adopt the assumption that $\theta/\omega_c \ll 1$, so the ratio ω_H/ω_L can be expanded in the order of θ/ω_c , and \mathcal{C}_{TL} ,

$$\mathcal{C}_{\text{TL}} = \exp \left(-\frac{1}{\phi_0^2} \frac{\hbar Z_T}{4\pi} \right) \left[1 + \frac{\theta}{\omega_c} + \frac{\theta^2}{2\omega_c^2} + o \left(\frac{\theta^3}{\omega_c^3} \right) \right]. \quad (\text{D15})$$

If we choose the characteristic impedance of the transmission line as $Z_T = 50 \Omega$. the lowest order approximation of the parameter \mathcal{C}_{TL} is 0.9961.

The second order term in the expansion of the coupling Hamiltonian is given by Eq. (D8b). Under the rotating wave approximation (and restoring dimensions), the second order term is

$$\begin{aligned} H_2/(-E_J \mathcal{C}_{\text{TL}} \mathcal{C}_c) &= - \left(\sum_k \frac{\tilde{\varphi}_T^2(k)}{2} (b_k^\dagger)^2 + \sum'_{k,q} \tilde{\varphi}_T(k) \tilde{\varphi}_T(q) b_k^\dagger b_q^\dagger \right) \sum_n \frac{(-1)^n \tilde{\varphi}_c^{2n+2}}{n! \cdot (n+2)!} (a^\dagger)^n a^{n+2} \\ &\quad - \left(\sum_k \frac{\tilde{\varphi}_T^2(k)}{2} b_k^2 + \sum'_{k,q} \tilde{\varphi}_T(k) \tilde{\varphi}_T(q) b_k b_q \right) \sum_n \frac{(-1)^n \tilde{\varphi}_c^{2n+2}}{n! \cdot (n+2)!} (a^\dagger)^{n+2} a^n \\ &\quad - \left(\sum_k \tilde{\varphi}_T^2(k) b_k^\dagger b_k + \sum'_{k,q} 2 \tilde{\varphi}_T(k) \tilde{\varphi}_T(q) b_k^\dagger b_q \right) \sum_n \frac{(-1)^n \tilde{\varphi}_c^{2n}}{(n!)^2} (a^\dagger a)^n. \end{aligned} \quad (\text{D16})$$

where the summation \sum' does not contain the terms that have the same indices.

Suppose the density operator of the cavity is given by $\rho(t)$ and the transmission line is assumed to be a vacuum bath. the master equation given by the nonlinear coupling Hamiltonian H_2 in Eq. (D16) is

$$\partial_t \rho(t) = -\frac{i}{\hbar} \text{Tr}_B [H_2(t), R(t_0)] - \frac{1}{\hbar^2} \text{Tr}_B \int_{t_0}^t [H_2(t), [H_2(\tau), R(\tau)]] d\tau \quad (\text{D17})$$

where R is the density operator for the system (cavity) and the bath (transmission line), which can be approximated by $R(t) \sim \rho(t) \otimes \rho_B$ and $\rho_B = |\text{vac}\rangle\langle\text{vac}|$ where $|\text{vac}\rangle$ is the vacuum state of the bath (transmission line). The partial trace of the bath DOFs is

$$\text{Tr}_B \{ \dots \} = \sum_{\{n_{k_1}, n_{k_2}, \dots\}} \langle n_{k_1}, n_{k_2}, \dots | \cdot | n_{k_1}, n_{k_2}, \dots \rangle \quad (\text{D18})$$

where $|n_{k_1}, n_{k_2}, \dots\rangle = |n_{k_1}\rangle |n_{k_2}\rangle \dots, |n_{k_i}\rangle$ is the n_{k_i} -photon Fock state of the mode $k = k_i$.

Note that because in H_2 , all the terms are aligned in the normal order, the first term in Eq. (D17) is zero. We will focus on the second term of Eq. (D17). After expansion of the commutation relation, the Eq. (D17) is

$$\begin{aligned} \dot{\rho} &= -\frac{1}{\hbar^2} \text{Tr}_B \int_{t_0}^t d\tau \{ H_2(t) H_2(\tau) \rho(\tau) \otimes \rho_B + \rho(\tau) \otimes \rho_B H_2(\tau) H_2(t) - H_2(t) \rho(\tau) \otimes \rho_B H_2(\tau) \\ &\quad - H_2(\tau) \rho(\tau) \otimes \rho_B H_2(t) \} \end{aligned} \quad (\text{D19})$$

Note that the Hamiltonian H_2 should be considered as the interaction picture Hamiltonian, where the transformation is $U = \exp(H_0)$, where H_0 is

$$H_0 = \hbar\omega_c a^\dagger a + \sum_k \hbar\omega_k b_k^\dagger b_k \quad (\text{D20})$$

Next, we will work term by term in Eq. (D19) to get master equation for the cavity field.

We start from the term

$$T_3 \equiv \frac{1}{\hbar^2} \int_{t_0}^t d\tau \text{Tr}_B \{ H_2(t) \rho(\tau) \otimes \rho_B H_2(\tau) \}. \quad (\text{D21})$$

As the transmission line is assumed to be a vacuum bath, and the coupling Hamiltonian H_2 is in normal order, the partial trace will kill all the terms that contain lowering operators for the bath DOFs. The Hamiltonian terms that survive in T_3 partial trace are

$$\frac{H_{2,1,(I)}(t)}{(E_J \mathcal{C}_{\text{TL}} \mathcal{C}_c)} \equiv h_{2,1,(I)}(t) = \sum_k h_{2,1,kk,(I)} + \sum'_{k,q} h_{2,1,kq,(I)} \quad (\text{D22a})$$

$$h_{2,1,kk,(I)}(t) = \frac{\tilde{\varphi}_T^2(k)}{2} (b_k^\dagger)^2 \hat{A}_2 e^{i2(\omega_k - \omega_c)t} \quad (\text{D22b})$$

$$h_{2,1,kq,(I)}(t) = \tilde{\varphi}_T(k) \tilde{\varphi}_T(q) b_k^\dagger b_q^\dagger \hat{A}_2 e^{i(\omega_k + \omega_q - 2\omega_c)t}, \quad (\text{D22c})$$

where the cavity nonlinear operator \hat{A}_2 is defined as

$$\hat{A}_2 = \sum_n \frac{(-1)^n \tilde{\varphi}_c^{2n+2}}{n! \cdot (n+2)!} (a^\dagger)^n a^{n+2} \quad (\text{D23})$$

and the Eq. (D21) is

$$\begin{aligned} \frac{T_3 \hbar^2}{(E_J \mathcal{C}_{\text{TL}} \mathcal{C}_c)^2} = \int_{t_0}^t d\tau \left\{ \sum_k \langle 2_k | h_{2,1,kk,(I)}(t) | \text{vac} \rangle \rho \langle \text{vac} | h_{2,1,kk,(I)}^\dagger(\tau) | 2_k \rangle \right. \\ \left. + \sum'_{k,q} \langle 1_k, 1_q | h_{2,1,kq,(I)}(t) | \text{vac} \rangle \rho \langle \text{vac} | h_{2,1,kq,(I)}^\dagger(\tau) | 1_k, 1_q \rangle \right\}, \end{aligned} \quad (\text{D24})$$

where we apply the bath state orthogonality relations and remove all the zero terms. Further, the term

$$\langle 2_k | h_{2,1,kk,(I)}(t) | \text{vac} \rangle = \frac{\sqrt{2} \tilde{\varphi}_T^2(k)}{2} \hat{A}_2 e^{i2(\omega_k - \omega_c)t} \quad (\text{D25a})$$

$$\langle 1_k, 1_q | h_{2,1,kq,(I)}(t) | \text{vac} \rangle = \tilde{\varphi}_T(k) \tilde{\varphi}_T(q) \hat{A}_2 e^{i(\omega_k + \omega_q - 2\omega_c)t} \quad (\text{D25b})$$

For the first term, which is involved in the time integral of the first line of Eq. (D24) (noted as $T_{3,1}$), after applying the Born-Markov approximation, and define $k_c = \omega_c/v_p$ and take Eq. (D13), the term $T_{3,1}$ is

$$T_{3,1} = (\mathcal{C}_{\text{TL}} \mathcal{C}_c)^2 \frac{E_J^2}{\hbar^2} \frac{l}{2\pi v_p} \int_{t_0}^t d\tau \int_{\omega_L}^{\omega_H} d\omega_k \frac{\tilde{\varphi}_T^4(k)}{2} \hat{A}_2 \rho(\tau) \hat{A}_2^\dagger e^{i2(\omega_k - \omega_c)t} \quad (\text{D26a})$$

$$= (\mathcal{C}_{\text{TL}} \mathcal{C}_c)^2 \frac{1}{8} \left(\frac{\hbar Z_T}{2\phi_0^2} \right) \frac{E_J^2}{\hbar^2 \omega_c} \tilde{\varphi}_T^2(k_c) \hat{A}_2 \rho(t) \hat{A}_2^\dagger \quad (\text{D26b})$$

$$= \Gamma_{2,1} \hat{A}_2 \rho(t) \hat{A}_2^\dagger. \quad (\text{D26c})$$

Similar to the definition of the nonlinear operator of the cavity field in first order coupling, we can redefine the nonlinear operator for second order as

$$\hat{A}'_2 = (\mathcal{C}_{\text{TL}} \mathcal{C}_c) \hat{A}_2 \quad (\text{D27})$$

and then the associated rate is

$$\hat{\Gamma}'_{2,1} = \frac{1}{(\mathcal{C}_{\text{TL}} \mathcal{C}_c)^2} \Gamma_{2,1} = \frac{1}{8} \left(\frac{\hbar Z_T}{2\phi_0^2} \right) \frac{E_J^2}{\hbar^2 \omega_c} \tilde{\varphi}_T^2(k_c) \quad (\text{D28})$$

Compared with the rate associated with the first order coupling Hamiltonian, Γ_1 [see Eq. (D12)], the rate associated with this term is

$$\Gamma'_{2,1}/\Gamma_1 = \frac{1}{8}\tilde{\varphi}_T^2(k_c). \quad (\text{D29})$$

For a realistic setup, where we assume the transmission is 1 m long, the cavity frequency is 7.5 GHz, and the speed of microwave along the transmission line is speed of light, and the characteristic impedance of the transmission line is 50 Ω , the quantization parameter $\tilde{\varphi}_T(k_c) \sim 0.0124$. So this process is much slower than the first order coupling, which is controlled by the small parameter $\tilde{\varphi}_T^2(k_c)$, which is equivalent to the small parameter $\frac{2\pi v_p}{\omega_c l}$ [see Eq. (D36)]. Especially, as the transmission line $l \rightarrow \infty$ (approaching theoretical limit), this term $\rightarrow 0$.

The second line of the Eq. (D24) (noted as $T_{3,2}$) is

$$T_{3,2} = (\mathcal{C}_{\text{TL}}\mathcal{C}_c)^2 \frac{E_J^2}{\hbar^2} \left(\sum_{k,q} - \sum_k \delta_{k,q} \right) \tilde{\varphi}_T^2(k) \tilde{\varphi}_T^2(q) \hat{A}_2 e^{i(\omega_k + \omega_q - 2\omega_c)(t-\tau)} \quad (\text{D30})$$

Note the second summation term is similar to the calculation in Eq. (D26), and it is $2\Gamma_{2,1}\hat{A}_2\rho(t)\hat{A}_2^\dagger$.

The first summation term

$$T_{3,2} + 2\Gamma_{2,1}\hat{A}_2\rho(t)\hat{A}_2^\dagger = (\mathcal{C}_{\text{TL}}\mathcal{C}_c)^2 \frac{E_J^2}{\hbar^2} \frac{l^2}{(2\pi v_p)^2} \int_{t_0}^t d\tau \int_{\omega_L}^{\omega_H} d\omega_k \int_{\omega_L}^{\omega_H} d\omega_q \left\{ \tilde{\varphi}_T^2(k) \tilde{\varphi}_T^2(q) \hat{A}_2 \rho(\tau) \hat{A}_2^\dagger e^{i(\omega_k + \omega_q - 2\omega_c)t} \right\} \quad (\text{D31})$$

With Born-Markov approximation, we replace $\tilde{\varphi}_T k$ and $\tilde{\varphi}_T q$ by the central frequency mode $k_c = \omega_k/v_p$, and because of the fast oscillation term $e^{i(\omega_k + \omega_q - 2\omega_c)t}$, only the modes that satisfies $\omega_k + \omega_q = 2\omega_c$ will have large contribution, we can approximate the integral of two modes frequencies by $\theta \int d\bar{\omega}$ where $\bar{\omega} = (\omega_k + \omega_q)/2$, and θ is the coupling bandwidth. Then the integral in Eq. (D31) is

$$T_{3,2} + 2\Gamma_{2,1}\hat{A}_2\rho(t)\hat{A}_2^\dagger = (\mathcal{C}_{\text{TL}}\mathcal{C}_c)^2 \frac{E_J^2}{\hbar^2} \frac{l^2 \theta}{(2\pi v_p)^2} \tilde{\varphi}_T^4(k_c) \int_{t_0}^t d\tau \int d\bar{\omega} \left\{ \hat{A}_2 \rho(\tau) \hat{A}_2^\dagger e^{2i(\bar{\omega} - \omega_c)t} \right\} \quad (\text{D32a})$$

$$= (\mathcal{C}_{\text{TL}}\mathcal{C}_c)^2 \frac{1}{4\pi} \left(\frac{\hbar Z_T}{2\phi_0^2} \right)^2 \frac{E_J^2}{\hbar^2} \frac{\theta}{\omega_c} \hat{A}_2 \rho(t) \hat{A}_2^\dagger \quad (\text{D32b})$$

$$\equiv \Gamma_{2,2} \hat{A}_2 \rho(t) \hat{A}_2^\dagger \quad (\text{D32c})$$

Note that this term is also slow compared to the first order dynamics. Similarly, to consistently compare with the first order rate in Eq. (D12), we redefine the cavity operator \hat{A} as Eq. (D27) and the rate associated rate $\Gamma'_{2,2}$ as

$$\Gamma'_{2,2} = \frac{1}{(\mathcal{C}_{\text{TL}}\mathcal{C}_c)^2} \Gamma_{2,2} = \frac{1}{4\pi} \left(\frac{\hbar Z_T}{2\phi_0^2} \right)^2 \frac{E_J^2}{\hbar^2} \frac{\theta}{\omega_c} \quad (\text{D33})$$

and then the ratio for the rates

$$\frac{\Gamma'_{2,2}}{\Gamma_1} = \frac{1}{4\pi} \left(\frac{\hbar Z_T}{2\phi_0^2} \right) \frac{\theta}{\omega_c}, \quad (\text{D34})$$

where if the transmission line impedance is 50 Ω , the term $\left(\frac{\hbar Z_T}{2\phi_0^2} \right) \sim 0.1560$ and in the quantum optics system assumption, $\theta/\omega_c \ll 1$. So this second order coupling dynamics is also slower than the first order coupling dynamics, and is controlled by the small parameter θ/ω_c .

Similarly, we can perform the same procedure for the other three terms and obtain the master equation induced by H_2

$$\partial_t \rho(t) = -\Gamma_2 \mathcal{D}[\hat{A}_2] \rho(t) \quad (\text{D35a})$$

$$\mathcal{D}[\hat{A}_2] \rho(t) = -\frac{1}{2} \left(\hat{A}_2^\dagger \hat{A}_2 \rho + \rho \hat{A}_2^\dagger \hat{A}_2 - 2\hat{A}_2 \rho(t) \hat{A}_2^\dagger \right) \quad (\text{D35b})$$

$$\hat{A}_2 = \mathcal{C}_{\text{TL}}\mathcal{C}_c \sum_n \frac{(-1)^n \tilde{\varphi}_c^{2n+2}}{n! \cdot (n+2)!} (a^\dagger)^n a^{n+2} \quad (\text{D35c})$$

$$\Gamma_2 = \left[\frac{1}{4\pi} \left(\frac{\hbar Z_T}{2\phi_0^2} \right)^2 \frac{E_J^2}{\hbar^2} \right] \left[\frac{\theta}{\omega_c} - \frac{\pi v_p}{2l\omega_c} \right] \quad (\text{D35d})$$

Finally, I want to note that the above derivation is valid when the length of the transmission line is large. This is consistent with the Born-Markov approximation. We assume in a coupling bandwidth $\theta \ll \omega_c$, the number of modes in this bandwidth is still much greater than the system DOFs, so the transmission line must be considered to be long, in which the integer

$$n_c \equiv \frac{k_c l}{2\pi} = \frac{\omega_c l}{2\pi v_p} \gg 1, \quad (\text{D36})$$

such that we can find an other integer n_θ which satisfies $|n_\theta - n_c| \gg 1$ and $n_\theta/n_c \ll 1$. In the regime where $l \rightarrow \infty$, the rate of the quantum process given by H_2 nonlinear system-bath coupling is given by $\Gamma'_{2,2}$ term [Eq. (D33)], and is controlled by small parameter θ/ω_c which does not depend on the length of the transmission line.

Similar to the discussion for the second order term in the ABOCC coupling circuit, after we apply the rotating-wave approximation, the third order Hamiltonian is given by

$$\frac{H_3}{E_J \mathcal{C}_c \mathcal{C}_{\text{TL}}} = i \left\{ \left(\sum_k \frac{\tilde{\varphi}_T^3(k)}{6} (b_k^\dagger)^3 + \sum_{k,q} \frac{\tilde{\varphi}_T(k) \tilde{\varphi}_T(q)}{2} (b_k^\dagger)^2 b_q^\dagger + \sum_{k,q,p} \tilde{\varphi}_T(k) \tilde{\varphi}_T(q) \tilde{\varphi}_T(p) b_k^\dagger b_q^\dagger b_p^\dagger \right) \right. \\ \left. \times \sum_n \frac{(-1)^n \tilde{\varphi}_c^{2n+3}}{n! \cdot (n+3)!} (a^\dagger)^n a^{n+3} - h.c. \right\} \quad (\text{D37a})$$

$$-i \left\{ \left[\sum_k \frac{\tilde{\varphi}_T^3(k)}{2} (b_k^\dagger)^2 b_k + \sum_{k,q} \tilde{\varphi}_T^2(k) \tilde{\varphi}_T(q) \left(b_q^\dagger b_k^\dagger b_k + \frac{1}{2} (b_k^\dagger)^2 b_q \right) \sum_{k,q,p} 6 \tilde{\varphi}_T(k) \tilde{\varphi}_T(q) \tilde{\varphi}_T(p) b_k^\dagger b_q^\dagger b_k \right] \right. \\ \left. \times \sum_n \frac{(-1)^n \tilde{\varphi}_c^{2n+1}}{n! \cdot (n+1)!} (a^\dagger)^n a^{n+1} - h.c. \right\} \quad (\text{D37b})$$

Follow the same argument in the discussion of the section order terms, the only Hamiltonian term that contributes to the system dynamics when the bath is in vacuum state is the first term in Eq. (D37a). We can define a system nonlinear operator

$$\hat{A}_3 = \mathcal{C}_c \mathcal{C}_{\text{TL}} \sum_n \frac{(-1)^n \tilde{\varphi}_c^{2n+3}}{n! \cdot (n+3)!} (a^\dagger)^n a^{n+3}. \quad (\text{D38})$$

In Eq. (D37a), there are three terms, the first term, $\sum_k \frac{\tilde{\varphi}_T^3(k)}{6} (b_k^\dagger)^3$ term, will give a Lindblad term in master equation of cavity field as $\mathcal{D}[\hat{A}_3]\rho(t)$ with rate $\Gamma_{3,1}$. This process is further suppressed by the small parameter $1/n_c$ [see Eq. (D36)] as

$$\frac{\Gamma_{3,1}}{\Gamma_1} \propto n_c^{-2} = \left(\frac{2\pi v_p}{\omega_c l} \right)^2. \quad (\text{D39})$$

The second term, $\sum_{k,q} (b_k^\dagger)^2 b_q^\dagger$ term, will give a Lindblad term $\mathcal{D}[\hat{A}_3]\rho(t)$ with rate $\Gamma_{3,2}$,

$$\frac{\Gamma_{3,2}}{\Gamma_1} \propto \frac{1}{n_c} \frac{\theta}{\omega_c} = \left(\frac{2\pi v_p}{\omega_c l} \right) \frac{\theta}{\omega_c}, \quad (\text{D40})$$

where θ is the coupling bandwidth. The third term $\sum_{k,q,p} b_k^\dagger b_q^\dagger b_p^\dagger$ gives the same Lindblad term with rate $\Gamma_{3,3}$,

$$\frac{\Gamma_{3,3}}{\Gamma_1} \propto \frac{\theta^2}{\omega_c^2}. \quad (\text{D41})$$

In the limit where $l \rightarrow \infty$, the third term is dominant, but is still further suppressed by θ/ω_c , even compared with the second order dynamics. In the main text, we ignore the second and third order terms in the system-bath coupling Hamiltonian and only focus on the first order terms.

[1] A. L. Schawlow and C. H. Townes, Phys. Rev. **112**, 1940 (1958).

- [2] L. Susskind and J. Glogower, *Physics Physique Fizika* **1**, 49 (1964).
- [3] S. Barnett, S. Stenholm, and D. Pegg, *Optics Communications* **73**, 314 (1989).
- [4] H. M. Wiseman, *Phys. Rev. A* **60**, 4083 (1999).
- [5] D. Gottesman, A. Kitaev, and J. Preskill, *Phys. Rev. A* **64**, 012310 (2001).
- [6] N. C. Menicucci, *Phys. Rev. Lett.* **112**, 120504 (2014).
- [7] K. Marshall, C. S. Jacobsen, C. Schäfermeier, T. Gehring, C. Weedbrook, and U. L. Andersen, *Nature Communications* **7**, 13795 (2016).
- [8] N. Didier, A. Kamal, W. D. Oliver, A. Blais, and A. A. Clerk, *Phys. Rev. Lett.* **115**, 093604 (2015).
- [9] A. Eddins, S. Schreppler, D. M. Toyli, L. S. Martin, S. Hacoheh-Gourgy, L. C. G. Govia, H. Ribeiro, A. A. Clerk, and I. Siddiqi, *Phys. Rev. Lett.* **120**, 040505 (2018).
- [10] C. M. Caves, *Phys. Rev. D* **23**, 1693 (1981).
- [11] R. S. Bondurant and J. H. Shapiro, *Phys. Rev. D* **30**, 2548 (1984).
- [12] Y. Ma, H. Miao, B. H. Pang, M. Evans, C. Zhao, J. Harms, R. Schnabel, and Y. Chen, *Nature Physics* **13**, 776 (2017).
- [13] X. Zuo, Z. Yan, Y. Feng, J. Ma, X. Jia, C. Xie, and K. Peng, *Phys. Rev. Lett.* **124**, 173602 (2020).
- [14] H. Yuen and J. Shapiro, *IEEE Transactions on Information Theory* **24**, 657 (1978).
- [15] R. E. Slusher and B. Yurke, *Journal of Lightwave Technology* **8**, 466 (1990).
- [16] D. Gottesman and J. Preskill, “Secure quantum key distribution using squeezed states,” in *Quantum Information with Continuous Variables*, edited by S. L. Braunstein and A. K. Pati (Springer Netherlands, Dordrecht, 2003) pp. 317–356.
- [17] H. Vahlbruch, M. Mehmet, S. Chelkowski, B. Hage, A. Franzen, N. Lastzka, S. Goßler, K. Danzmann, and R. Schnabel, *Phys. Rev. Lett.* **100**, 033602 (2008).
- [18] S. Bartalini, S. Borri, P. Cancio, A. Castrillo, I. Galli, G. Giusfredi, D. Mazzotti, L. Gianfrani, and P. De Natale, *Phys. Rev. Lett.* **104**, 083904 (2010).
- [19] J. G. Bohnet, Z. Chen, J. M. Weiner, D. Meiser, M. J. Holland, and J. K. Thompson, *Nature* **484**, 78 (2012).
- [20] Y. Yamamoto, S. Machida, and O. Nilsson, *Phys. Rev. A* **34**, 4025 (1986).
- [21] H. Walther, B. T. Varcoe, B.-G. Englert, and T. Becker, *Reports on Progress in Physics* **69**, 1325 (2006).
- [22] S. M. Girvin, *Circuit QED: superconducting qubits coupled to microwave photons* (Oxford University Press, 2014).
- [23] V. E. Manucharyan, J. Koch, L. I. Glazman, and M. H. Devoret, *Science* **326**, 113 (2009).
- [24] J. Koch, T. M. Yu, J. Gambetta, A. A. Houck, D. I. Schuster, J. Majer, A. Blais, M. H. Devoret, S. M. Girvin, and R. J. Schoelkopf, *Phys. Rev. A* **76**, 042319 (2007).
- [25] J. A. Schreier, A. A. Houck, J. Koch, D. I. Schuster, B. R. Johnson, J. M. Chow, J. M. Gambetta, J. Majer, L. Frunzio, M. H. Devoret, S. M. Girvin, and R. J. Schoelkopf, *Phys. Rev. B* **77**, 180502 (2008).
- [26] A. A. Clerk, M. H. Devoret, S. M. Girvin, F. Marquardt, and R. J. Schoelkopf, *Rev. Mod. Phys.* **82**, 1155 (2010).
- [27] N. Bergeal, F. Schackert, M. Metcalfe, R. Vijay, V. Manucharyan, L. Frunzio, D. Prober, R. Schoelkopf, S. Girvin, and M. Devoret, *Nature* **465**, 64 (2010).
- [28] O. Astafiev, K. Inomata, A. O. Niskanen, T. Yamamoto, Y. A. Pashkin, Y. Nakamura, and J. S. Tsai, *Nature* **449**, 588 (2007).
- [29] F. Chen, J. Li, A. D. Armour, E. Brahim, J. Stettenheim, A. J. Sirois, R. W. Simmonds, M. P. Blencowe, and A. J. Rimberg, *Phys. Rev. B* **90**, 020506 (2014).
- [30] C. Rolland, A. Peugeot, S. Dambach, M. Westig, B. Kubala, Y. Mukharsky, C. Altimiras, H. le Sueur, P. Joyez, D. Vion, P. Roche, D. Esteve, J. Ankerhold, and F. Portier, *Phys. Rev. Lett.* **122**, 186804 (2019).
- [31] M. C. Cassidy, A. Bruno, S. Rubbert, M. Irfan, J. Kamhuber, R. N. Schouten, A. R. Akhmerov, and L. P. Kouwenhoven, *Science* **355**, 939 (2017).
- [32] S. H. Simon and N. R. Cooper, *Phys. Rev. Lett.* **121**, 027004 (2018).
- [33] D. K. L. Oi, V. Potoček, and J. Jeffers, *Phys. Rev. Lett.* **110**, 210504 (2013).
- [34] L. C. G. Govia, E. J. Pritchett, and F. K. Wilhelm, *New Journal of Physics* **16**, 045011 (2014).
- [35] S. Rosenblum, O. Bechler, I. Shomroni, Y. Lovsky, G. Guendelman, and B. Dayan, *Nature Photonics* **10**, 19 (2016).
- [36] M. Um, J. Zhang, D. Lv, Y. Lu, S. An, J.-N. Zhang, H. Nha, M. S. Kim, and K. Kim, *Nature Communications* **7**, 11410 (2016).
- [37] J. C. J. Radtke, D. K. L. Oi, and J. Jeffers, *Journal of Physics B: Atomic, Molecular and Optical Physics* **50**, 215501 (2017).
- [38] R. Ma, B. Saxberg, C. Owens, N. Leung, Y. Lu, J. Simon, and D. I. Schuster, *Nature* **570**, E52 (2019).
- [39] M. Mucci, X. Cao, C. Liu, R. Kaufman, D. Pekker, and M. Hatridge (APS, 2020).
- [40] H. M. Wiseman, S. N. Saadatmand, T. J. Baker, and D. W. Berry, in *Rochester Conference on Coherence and Quantum Optics (CQO-11)* (Optical Society of America, 2019) p. M3A.1.
- [41] T. J. Baker, S. N. Saadatmand, D. W. Berry, and H. M. Wiseman, “The heisenberg limit for laser coherence,” (2020), arXiv:2009.05296.
- [42] M. O. Scully and M. S. Zubairy, *Quantum Optics* (Cambridge University Press, 1997).
- [43] C. Gardiner, P. Zoller, and P. Zoller, *Quantum Noise: A Handbook of Markovian and Non-Markovian Quantum Stochastic Methods with Applications to Quantum Optics*, Springer Series in Synergetics (Springer, 2004).
- [44] H.-J. Briegel and B.-G. Englert, *Phys. Rev. A* **47**, 3311 (1993).
- [45] C. Ginzler, H.-J. Briegel, U. Martini, B.-G. Englert, and A. Schenzle, *Phys. Rev. A* **48**, 732 (1993).
- [46] H.-J. Briegel, B.-G. Englert, C. Ginzler, and A. Schenzle, *Phys. Rev. A* **49**, 5019 (1994).
- [47] Here there will be another factor of 2, which is because of the coupling to the left-propagating modes and the right-propagating modes.